Design and application of soy protein isolate films reinforced with Janus nanoparticles for active packaging of minced meat

Roghayieh Razavi[1], Mehran Moradi[1,*], Hossein Tajik[1], Rahim Molaei[2,*]

[1]Department of Food Hygiene and Quality Control, Faculty of Veterinary Medicine, Urmia University, Urmia, Iran; [2]Materials Synthesis Laboratory, Carbon Tech Industrial Group, Carbon Tech, Urmia, Iran

***Corresponding Authors:** Mehran Moradi, Department of Food Hygiene and Quality Control, Faculty of Veterinary Medicine, Urmia University, Urmia, Iran. Emails: moradi.mehran@yahoo.com, m.moradi@urmia.ac.ir; Rahim Molaei, Synthesis Laboratory, Carbon Tech Industrial Group, Carbon Tech, Urmia, Iran; Email: rahimmolaie@yahoo.com

Academic Editor: Gulden Goksen: Department of Food Technology, Vocational School of Technical Sciences at Mersin Tarsus Organized Industrial Zone, Tarsus University, 33100, Mersin, Türkiye

Received: 8 November 2025; Accepted: 5 May 2026; Published: 29 May 2026

ORIGINAL ARTICLE

Abstract

This study aimed to develop active soy protein isolate (SPI)-based packaging films incorporating Janus nanoparticles (JNPs) to improve the shelf life of minced meat. JNPs were synthesized using carboxymethyl cellulose and beeswax-based hydrophobic carbon dots and incorporated into SPI films at 0.03, 0.05, and 0.1% (w/w). Films were characterized for microstructure, antibacterial and antioxidant activities, mechanical properties, color, release pattern, and UV-blocking properties. FTIR and FESEM confirmed the homogeneous dispersion of JNPs. SPI-JNP0.1% films exhibited improved tensile strength (15.2 MPa vs. 9.6 MPa in SPI film) and elastic modulus (175.7 MPa vs. 112.5 MPa in SPI film), with slightly reduced elongation (31.4% vs. 36.5% in SPI film). Release studies showed that JNPs diffusion into food simulants was concentration-dependent. Antibacterial tests revealed superior inhibition of *Listeria monocytogenes*. When applied to beef, SPI-JNP films (0.1%) reduced total mesophilic and psychrotrophic counts by 4.4 and 4.2 $\log_{10}$ CFU/g after 9 days at 7 °C. These results highlight the potential of JNPs as functional nanofillers in biodegradable food packaging.

Keywords: active packaging; Janus nanoparticles; minced meat; soy protein isolate

Introduction

The spoilage of meat products within the food supply chain is attributed to their high content of polyunsaturated fatty acids, combined with low oxidative stability and heightened vulnerability to microbial growth (Ghorbani *et al*., 2024). Grinding also destroys muscle structural integrity, creating an unstable food matrix that favors both microbial spoilage and enzymatic and chemical oxidation reactions, potentially compromising meat safety. In the past decades, various techniques have been proposed to address these limitations and increase the shelf life of meat products, including thermal and non-thermal technologies and active and intelligent packaging (Roila *et al*., 2022).

Plastics derived from petroleum are widely used as packaging materials for food, causing enormous environmental issues and adulterating food with microplastics, which subsequently increase the risk of cancer in humans (Ahmed *et al*., 2022). The aforementioned constraints can be addressed through green packaging

based on natural biopolymers, including polysaccharides and proteins, which are biodegradable, non-toxic, and have negligible environmental effects (Hadavifar *et al.*, 2025). Soy protein isolate (SPI), a by-product of defatted soybeans, has gained significant interest as a film-forming biopolymer due to its excellent film-forming capacity, edibility, biodegradability, and wide availability (Akrami *et al.*, 2023). Nevertheless, SPI films have some limitations, including poor water resistance, low mechanical strength, and insufficient active functionality necessary for their effective application in food packaging (Akrami *et al.*, 2023; Hadavifar *et al.*, 2025).

To enhance SPI film properties, recent studies have incorporated various novel biomaterials, including carbon dots (CDs), nanoparticle composites (e.g., Ag-CDs and TiO_2), plant extracts (e.g., anthocyanin, *Ziziphora*, and mangosteen peel extract), and natural oils (e.g., black seed oil) (Huang *et al.*, 2021; Koshy *et al.*, 2022; Yavari Maroufi *et al.*, 2023; Hosseiniyeh *et al.*, 2024). CDs present special opportunities for the development of active and multifunctional materials used in food packaging. This is attributed to their functional properties, structural features, and the tunability of these characteristics during synthesis, which collectively offer significant advantages for antimicrobial food packaging applications (Lin *et al.*, 2022). In spite of their wide-ranging industrial uses, some drawbacks, such as toxicity, color alteration, and various odors, have restricted their application in food-related applications (Madannejad *et al.*, 2019). Several approaches have been suggested to overcome these limitations, such as minimizing the use of brown-colored CDs in foods (Kumar and Gaikwad, 2023) a and their concurrent application in combination with other alternative antibacterial substances, such as postbiotics (Divsalar *et al.*, 2025) and essential oils (Sattariazar *et al.*, 2023). CDs with improved functionality, nonetheless, could be developed through structural modification (Molaei *et al.*, 2025). As an advanced form of structural modification, the engineering of CDs into asymmetric Janus architectures presents a promising strategy to overcome these inherent drawbacks. Janus particles, which draw their name from Janus, the two-faced Roman deity, represent a distinctive class of particles characterized by two separate regions and properties (Yuan *et al.*, 2024).

Our previous research demonstrated that Janus nanoparticles (JNPs) developed using CDs and cellulose materials had lower toxicity than the original CDs while maintaining antimicrobial and antioxidant properties (Razavi *et al.*, 2024). This has facilitated the development of nanomaterials with improved functionalities and a reduced required dosage in food applications. JNPs, nanostructures with dual chemical or physical functionalities on opposite faces, offer unique opportunities for the design of multifunctional food packaging materials owing to their amphiphilic nature, interfacial activity, and tunable interactions (Wang *et al.*, 2023). This distinctive morphology enables JNPs to function across multiple environments, making them highly versatile for various applications, particularly in food packaging (Liu *et al.*, 2022). To date, little research has been conducted on the use of JNPs in active food packaging. Alizadeh *et al.* (2026) prepared antibacterial films based on JNPs and bacterial nanocellulose and evaluated their potential to inhibit *Salmonella Typhimurium* growth in chicken breast meat during cold storage. Fan *et al.* (2025) fabricated a Janus-structured film combining zein/chitosan and incorporated a co-loaded tannic acid and cinnamon essential oil Pickering emulsion. They evaluated its effectiveness as an antimicrobial packaging material for pork preservation. In another study, Zhu *et al.* (2024) developed a chitosan/polycaprolactone-thymol Janus film, which effectively maintained the quality of pork and prolonged its shelf life. Xue *et al.* (2024) developed a Janus hydrogel system using sodium alginate, trehalose, cinnamon essential oil, microcapsules of $NaHCO_3$, and citric acid in order to preserve various fruits and vegetables by exerting antioxidant properties, protecting color, and inhibiting microbial growth. Similarly, Yuan *et al.* (2024) also developed a Janus composite coating using chitosan and aldehyde carboxycellulose nanofibers for application in mangoes, bananas, and loquats. The outer chitosan layer served as an antibacterial layer, extending fruit freshness by 5–10 days. However, the potential of JNPs as a functional filler in food-grade biopolymers and SPI-based active packaging, specifically for prolonging the shelf life of perishable meat products, has not been investigated. To date, no systematic studies have examined how JNPs interact with plant protein-based films or how such incorporation influences film structure, barrier properties, mechanical strength, and antimicrobial efficacy.

This study aimed to fill this gap by developing a green and functional packaging material made of SPI with JNPs to improve the safety and shelf life of meat products. We hypothesized that the dual structure of JNPs would enable seamless integration into the SPI matrix. The hydrophobic side is expected to interact with the exposed hydrophobic regions of the denatured protein, thereby enhancing mechanical strength. Simultaneously, the hydrophilic side will improve dispersion and stability via hydrogen bonding. This synergistic interaction is anticipated to yield a film with superior mechanical properties, improved elasticity, and inherent antimicrobial activity. Physical, chemical, and mechanical analyses were conducted to understand the effects of incorporating JNPs into the biopolymer-based packaging system.

Materials and Methods

Materials

Soy protein isolate (SPI) (protein content >92%) and glycerol were purchased from Sigma-Aldrich, Germany. Bacterial strains were obtained from the Iranian Research Organization for Science and Technology. This study used Mueller–Hinton agar and plate count agar (PCA) from Ibresco Company, Tehran, Iran; 2-thiobarbituric acid; and Tryptic Soy Broth (TSB) from Quelab, Montreal, Canada. DPPH and trichloroacetic acid (TCA) were obtained from Sigma-Aldrich (Madrid, Spain). Deionized water (DW) was supplied by Diofaw, Urmia, Iran, and ethanol was acquired from Pars Alcohol (Shiraz, Iran). Other compounds and reagents used in this study were provided by Merck, Darmstadt, Germany.

JNPs synthesis

JNPs were synthesized in a two-step process. First, hydrophobic CDs were prepared via a hydrothermal method: 5 g of beeswax was dispersed in 80 mL of acetic acid, stirred for 1 h, transferred into a 250 mL Teflon-lined autoclave, and placed in a hot air oven at 200 °C for 10 h. The reactor filling ratio was approximately 40% (v/v), with a remaining headspace of ~60%. After the reaction, the autoclave was cooled naturally to room temperature (25 °C) without forced cooling. The heating rate was not monitored during this step. The product was purified by adding it to 300 mL of boiled deionized water, filtering it through Whatman No. 42 paper, and dispersing the filtrate in diethyl ether to separate the hydrophobic phase. The CD powder was collected by solvent evaporation at 35 °C. In the second step, these CDs were dissolved in 10% (v/v) DMSO and mixed with a 0.5% (w/v) CMC solution at a 2:1 volume ratio and stirred at 650 rpm and 25 °C for 48 h, followed by freeze-drying (freezing at −40 °C, shelf temperature −60 °C, pressure 100 mTorr) to obtain the final JNPs powder, which was stored at 22 ± 1 °C for characterization (Razavi *et al*., 2024).

Film preparation

The film-casting method was used for film preparation, as explained by Hosseiniyeh *et al*. (2024). SPI-JNPs and SPI-CDs films were prepared by dissolving SPI in water (4%), adjusting the pH to 10.5, heating at 70 °C for 45 min, and adding glycerol (35% w/w) as a plasticizer. Afterwards, JNPs and beeswax-based hydrophobic CDs were added separately to the SPI solution under magnetic stirring until the solution became homogeneous. The resultant solution (approx. 100 mL) was cast onto a Teflon-coated glass plate and dried at 28 °C for 48 h. The films were peeled off and conditioned at 25 °C and 50% RH for 48 h before testing.

Films characterization

FESEM and FTIR analysis

The surface morphologies of the SPI-JNP and SPI-CD films were investigated using field-emission scanning electron microscopy (FESEM; SIGMA VP-500; Zeiss, Germany). The chemical structures of the films were characterized using Fourier-transform infrared spectroscopy (FTIR; Thermo Electron, Nexus® 670, Madison, USA) within the range of 450–4000 cm^{-1}, with a resolution of 4 cm^{-1}.

Color UV-Vis blocking properties

The color attributes (L^*, a^*, and b^*) of the SPI films were measured using a Lovibond® LC 100 spectrocolorimeter (Tintometer® Group, Lovibond House, UK). The total color difference (ΔE) between the films was determined using Eq. (1):

$$\Delta E = \sqrt{(L^*-L_o^*) + (a^*-a_o^*) + (b^*-b_o^*)}, \quad \text{Eq. (1)}$$

where L_0^* (97.12), a_0^* (−0.14), and b_0^* (0.13) represent the colorimetric parameters of the standard paper and L^*, a^*, and b^* denote the values of the film.

The UV-barrier properties of the SPI-JNP and SPI-CD films were assessed using a double-beam spectrophotometer (T80+ UV–Vis spectrophotometer PG, Beijing, China). The film samples were positioned in the spectrophotometer sample holder to determine their light transmittance, with a resolution of 1 nm across the wavelength range of 200–900 nm (Yuan *et al*., 2024). Air was used as the reference baseline for calibration at 100% transmittance.

Mechanical properties

The thickness of the SPI-CDs, SPI-JNP, and SPI films was determined using a digital micrometer (Fowler, USA) with an accuracy of 0.01 mm at five random points on each film sample. The mean thickness obtained from these measurements was used to calculate the mechanical properties (Hosseiniyeh *et al*., 2024). The tensile strength (TS; MPa) and elongation at break (EAB; %) of the SPI-JNP and SPI-CD films were measured using a universal testing instrument (Santam, Tehran, Iran) at a crosshead speed of 5 mm/min and a gauge length of 50 mm. Prior to testing, the films were conditioned at 25 °C and 50% RH for 48 h (ASTM, 2012).

Release behavior

The release patterns of JNPs and CDs from the SPI films were assessed using food simulants, as outlined by Razavi *et al*. (2020). Ethanol solutions of 10, 50, and 95% were prepared to simulate aqueous foods, oil-in-water emulsions, and fatty foods, respectively. Square samples (1.5 × 1.5 cm) of the films prepared at three different concentrations (0.03, 0.05, and 0.1%) were placed in flasks containing 20 mL of each simulant. Samples were incubated at 25 °C with shaking at 90 rpm for 48 h. Absorbance at 280 nm was measured at predetermined time intervals. The percentage of release was calculated using Eq. (2) *(*Meerasri *et al*., 2024):

$$Release\ (\%) = \frac{Mt}{M} \times 100 \qquad \text{Eq. (2)}$$

Mt represents the amount of JNPs or CDs released from the SPI films at time t (min), and M represents their initial concentration in the SPI films. JNPs release was quantified using UV–Vis spectroscopy at 280 nm. A calibration curve was established using standard JNPs solutions (0–0.6 mg/mL), yielding a linear relationship described by the equation y = 3.0793x + 0.1457, with a correlation coefficient (R^2) of 0.9913. The calibration curve is provided in the Supplementary Material (Figure S1). These data were used to convert absorbance readings to concentration values for release calculations.

Antioxidant activity

The 2,2-diphenyl-1-picrylhydrazyl (DPPH) radical scavenging activity of SPI-CDs and SPI-JNP films was determined (Hosseiniyeh *et al*., 2024). In brief, 25 mg of each film was dissolved in 4 mL of DW. Then, 2 mL of the film extract solution was added to 200 µL of DPPH solution (1 mM in methanol). The resulting solutions were kept in darkness at ambient temperature for 60 min. Absorbance was measured at 517 nm using a UV–visible spectrophotometer. The radical scavenging percentage (% RS) was estimated using Eq. (3).

$$\%RS = \{ (A_{blank} - A_{sample})/A_{blank} \} \times 100 \qquad \text{Eq. (3)}$$

where A_{blank} and A_{sample} represent the absorbance of the DPPH solution and the DPPH solution containing film extract, respectively.

The antioxidant potential of the films to reduce Fe^{3+} into Fe^{2+} was evaluated using the FRAP assay. In brief, a FRAP reagent was prepared as a mixture of 0.3 M acetate buffer (pH 3.6), 20 mM ferric chloride ($FeCl_3 \cdot 6H_2O$) solution, and 10 mM TPTZ in 40 mM HCl, in a 10:1:1 ratio. The film extract solution (150 µL) was mixed with the FRAP solution (2850 µL) and incubated in the dark at 23 ± 1 °C for 30 min. Then, the absorbance at 593 nm was measured using a spectrophotometer (Adilah *et al*., 2018).

Antimicrobial activity

The antibacterial properties of the films were assessed through the agar-diffusion technique. Mueller–Hinton agar plates were seeded with 10^8 CFU/mL of *Escherichia coli* O157:H7 (PTCC 1399) and *Listeria monocytogenes* (PTCC 1298). Discs of SPI-CD and SPI-JNP films (0.03, 0.05, and 0.1%) with a diameter of 8 mm were sterilized using UV light for 2 min, then positioned in the center of an agar plate and incubated at 37 ± 1 °C for 24 h. The size of the inhibition zone was measured (Nikfarjam *et al*., 2025).

The antibacterial effect was assayed using the shaking flask method (Li *et al*., 2014). Two milliliters of each calibrated bacterial suspension (6 $\log_{10}$ CFU/mL) were transferred to tubes containing 18 mL of sterile TSB. Sterilized films of SPI-JNP and SPI-CD, with dimensions of 1.5 × 1.5 cm and concentrations of 0.03, 0.05, and 0.1%, were introduced into the tubes. A control group was set up with tubes containing only bacteria and culture medium. The tubes were incubated in a shaker at 100 rpm and kept at 37 °C for 24 h. Bacterial counts were monitored spectrophotometrically at 600 nm at 0, 4, 8, 12, and 24 h. Blank samples consisted of tubes containing SPI film samples without bacterial suspensions. Antibacterial activity (%) was calculated using Eq. (4), based on the optical density difference between the control (A) and treated samples (B).

$$Antibacterial\ activity\ (\%) = \left\{ \frac{A - B}{A} \right\} \times 100 \qquad \text{Eq. (4)}$$

Meat application

Fresh minced beef was purchased from a local market in Urmia, Iran, and transferred to the food packaging laboratory under hygienic conditions. Portions of 40 g minced beef were aseptically sandwiched between two identical film pieces. Meat samples were assigned to eight groups based on their packaging: an unwrapped control group, a group wrapped with pure SPI film, and groups wrapped with SPI-based active films. The active films, SPI-JNP and SPI-CD, were selected for their non-toxic and strong antibacterial properties, each at three

concentrations (0.03, 0.05, and 0.1%). Each sample was individually packaged and stored at 7 ± 1 °C for 9 days. The following tests and analyses were conducted at 0, 3, 6, and 9 days (Shafipour Yordshahi *et al*., 2020).

Microbial analysis

Based on the method described by Razavi *et al*. (2024), the total mesophilic bacteria count (TMBC) was measured using the pour plate method, while the total psychrophilic bacteria count (TPBC) was determined using the surface-spread technique.

Physico-chemical analysis

The pH was determined using a digital pH meter (Metrohm, Herisau, Switzerland). The meat samples were analyzed for total volatile basic nitrogen (TVB-N) (mg N/100 g) using a Kjeldahl distillation apparatus, following the method described by Mirmoeini *et al*. (2023). Ten grams of the meat sample were mixed with 300 mL of DW. After adding 2 g of MgO, the homogenate was transferred to a Kjeldahl flask and heated. The distillate was collected over 25 min in a receiving flask containing 25 mL of boric acid solution (2% v/v) and a few drops of methyl red (0.1%) and methylene blue (0.1%) as indicators. The distillate was then titrated with 0.1 N sulfuric acid. TVB-N content was calculated using Eq. (5) and expressed as mg/100 g:

$$\text{TVB-N content: mg/100 g} = V_1\,(\text{mL}) \times 14 \qquad \text{Eq. (5)}$$

Where V_1 is the volume of sulfuric acid used in the titration.

The thiobarbituric acid reactive substances (TBARS) assay was used to estimate lipid oxidation in the samples (Semsari *et al*., 2024). Briefly, meat samples (10 g) were homogenized with BHT solution (1 mg/mL) and TCA solution (35 mL, 4%), filtered through Whatman No. 42 filter paper, and adjusted to a final volume of 50 mL with the same TCA solution. The filtrate (5 mL) was mixed with TBA reagent (10 mL, 0.02 M), and the mixture was incubated at 90 °C for 1 h. Absorbance measurements at 532 nm were performed spectrophotometrically, with a blank consisting of 2 mL of 0.02 M TBA and 2 mL of 4% TCA. The concentration of malondialdehyde (MDA) in each sample was calculated using a standard curve.

Sensory evaluation

Sensory attributes, including odor, color, and overall acceptability, were evaluated using a 9-point hedonic scale ranging from 1 (dislike extremely) to 9 (like extremely). A panel of 12 semi-trained panelists (four males and eight females; 26–40 years old) analyzed each coded sample using a form with a quantitative rating scale in separate chambers under incandescent lighting at 28 ± 1 °C and 60% humidity (Razavi *et al*., 2024). In the absence of a human ethics committee or a formal documentation process, the authors assure that all necessary steps were taken to protect the rights and privacy of participants throughout the study. They also confirm that informed consent was obtained from each participant before participation in the research. At the start of each evaluation session, two reference samples were provided to each panelist: a control (standard formulation) as a baseline and a blind-coded replicate from the test samples. Panelists recorded their ratings for these references before assessing the main samples to calibrate their mental scale for each session. Color attributes of the samples were measured three times using a Lovibond® LC 100 spectrocolorimeter.

Statistical analysis

Each experiment was performed three times, and ANOVA (GraphPad Prism, version 8.01 for Windows; GraphPad Software Inc., San Diego, CA, USA) was used to analyze the data. Significant differences ($p < 0.05$) were identified using Tukey's post hoc test. Principal component analysis (PCA) was conducted using the 'factoextra' package in R software (version 4.2.2) on a dataset comprising the following measured variables: pH, TVB-N, TBARS, TMBC, TPBC, and the sensory attributes of color, odor, and overall acceptance.

Results and Discussion

JNPs synthesis

The Janus architecture of the NPs has been previously confirmed using complementary techniques, including transmission electron microscopy (TEM), particle size analysis, and zeta potential measurements (Razavi *et al*., 2024), which suggested the presence of dual-functional domains. The synthesized hydrophobic CDs were characterized as small, spherical particles with an average diameter of 2.4 nm, as determined by a scatteroscope particle size analyzer (PSA, Qudix Inc., South Korea) at 23 ± 1 °C, with over 99% of the particles measuring below 5 nm (Razavi *et al*., 2024). TEM imaging confirmed their well-dispersed, spherical morphology (<10 nm) and the absence of aggregation. They exhibited a zeta potential of −21 mV, indicating good colloidal stability. The derived JNPs had an average diameter of 3.99 nm, with over 99% of

the particles below 10.8 nm. FESEM imaging revealed an approximately spherical morphology with a rough surface for the JNPs.

Chemical structure and morphology of films

FTIR spectroscopy was performed on the SPI, SPI-CD, and SPI-JNP films (Figure 1). As shown in Figure 1A, the functional groups identified in the SPI film were hydroxyl (O–H) and amine (N–H) groups, observed as a strong transmission band at 3277 cm^{-1}. Additionally, the C=O stretching of the primary amide group appeared at 1636 cm^{-1}, while the N–H bending vibrations and C–N stretching vibrations at 1538 cm^{-1} and 1405 cm^{-1}, respectively, were attributed to the secondary amide. The peak at 2930 cm^{-1} was attributed to C–H stretching vibrations of the soy protein isolate. The absorption bands observed between 1238 and 1402 cm^{-1} are characteristic of amide III vibrations arising from C–N stretching with N–H bending modes (Hosseiniyeh *et al*., 2024). Furthermore, the transmission band at 1038 cm^{-1} was assigned to C–O stretching vibrations from carbohydrate components associated with the SPI (Guerrero *et al*., 2013). Comparison of the FTIR spectra revealed minor shifts in the amide I band upon CD incorporation (from 1636 to 1644 cm^{-1}), along with corresponding minor shifts from 3277 cm^{-1} to 3279 cm^{-1} and from 1038 cm^{-1} to 1035 cm^{-1}. These subtle shifts suggest the presence of weak physical interactions, such as hydrogen bonding, between the functional groups of the CDs and the protein matrix. The surface functionality of CDs plays an important role in their interaction with biopolymers. Rani *et al*. (2020), in examining the spectra of soy protein films containing CDs, reported that amine-functionalized CDs caused a shift in the amide II band from 1544 to 1530 cm^{-1}, suggesting the formation of chemical interactions. In contrast, carboxyl-functionalized CDs generated a new peak at 1741 cm^{-1}, indicating the presence of free carboxyl groups and the absence of strong chemical interactions with the protein matrix. The FTIR spectrum of the SPI-JNP film (Figure 1C) revealed a distinct interaction pattern. While the critical amide I band remained unshifted at 1636 cm^{-1}, offering strong evidence against covalent bond formation, a distinct shift in the amide II band from 1538 cm^{-1} (pristine SPI) to 1550 cm^{-1} was observed. This shift, accompanied by a slight broadening of the broad O–H/N–H band around 3277 cm^{-1}, indicates a modification in the hydrogen-bonding network and the local environment of the N–H groups within the protein matrix. The absence of any new vibrational modes suggests that no new chemical bonds were formed. This spectral pattern indicates that JNPs integrate into the SPI matrix through strong physical interactions (e.g., hydrogen bonding and electrostatic forces) that perturb the protein's physical network without altering its core chemical structure.

The spectral similarity among all SPI-based films suggests a high degree of compatibility between JNPs and the SPI matrix, as evidenced by the overlapping characteristic bands of O–H, C–H, and N–H functional groups (Hadavifar *et al*., 2025). These results collectively suggest a predominantly physical interaction between JNPs and the SPI matrix, indicating that, while the chemical structure remains intact, the physical organization and microstructure of the polymer network are modified. This finding is consistent with the results reported by Hosseiniyeh *et al*. (2024). In their study on SPI films incorporated with black seed oil nanoemulsion, no new peaks emerged in the 4000–500 cm^{-1} range, indicating that the primary functional groups of the protein remained intact after modification.

Additionally, Figure 1F displays the impact of CDs and JNPs on the morphological characteristics and structural features of SPI films. In the present study, FESEM analysis was primarily used to evaluate particle dispersion within the film matrix rather than to independently confirm the anisotropic morphology of JNPs. The dense, smooth, and continuous surface of the SPI film reflects its good film-forming capacity (Hu *et al*., 2023). Following the incorporation of CDs, the film surface lost its uniformity, and roughness appeared in the form of localized aggregates in some regions (Figure 1G). This is primarily attributed to the inherent incompatibility between the hydrophobic CDs and the hydrophilic SPI matrix. This incompatibility reduces interfacial interaction energy, ultimately driving phase separation and CD agglomeration to minimize hydrophobic–hydrophilic contact (Shang *et al*., 2018). As anticipated for film samples containing hydrophobic compounds, surface roughness was observed, as reported by Hosseiniyeh *et al*. (2024). This was explained by the reduced tendency of hydrophobic CDs to blend with the protein matrix. In contrast, the JNPs were evenly distributed throughout the SPI film without significant aggregation (Figure 1H). This homogeneous dispersion can be attributed to the dual structure of JNPs and the hydrophilic nature of these particles. Their hydrophilic moiety integrates favorably with the hydrophilic SPI matrix, while their hydrophobic moiety is accommodated within the film structure, preventing large-scale phase separation. These findings are consistent with the established principle that surface compatibility governs nanoparticle dispersion in polymer matrices. This has been demonstrated in various composite systems containing hydrophilic nanofillers in protein films (Koshy *et al*., 2022). The absence of complementary characterization techniques, such as XRD and DSC, is a limitation

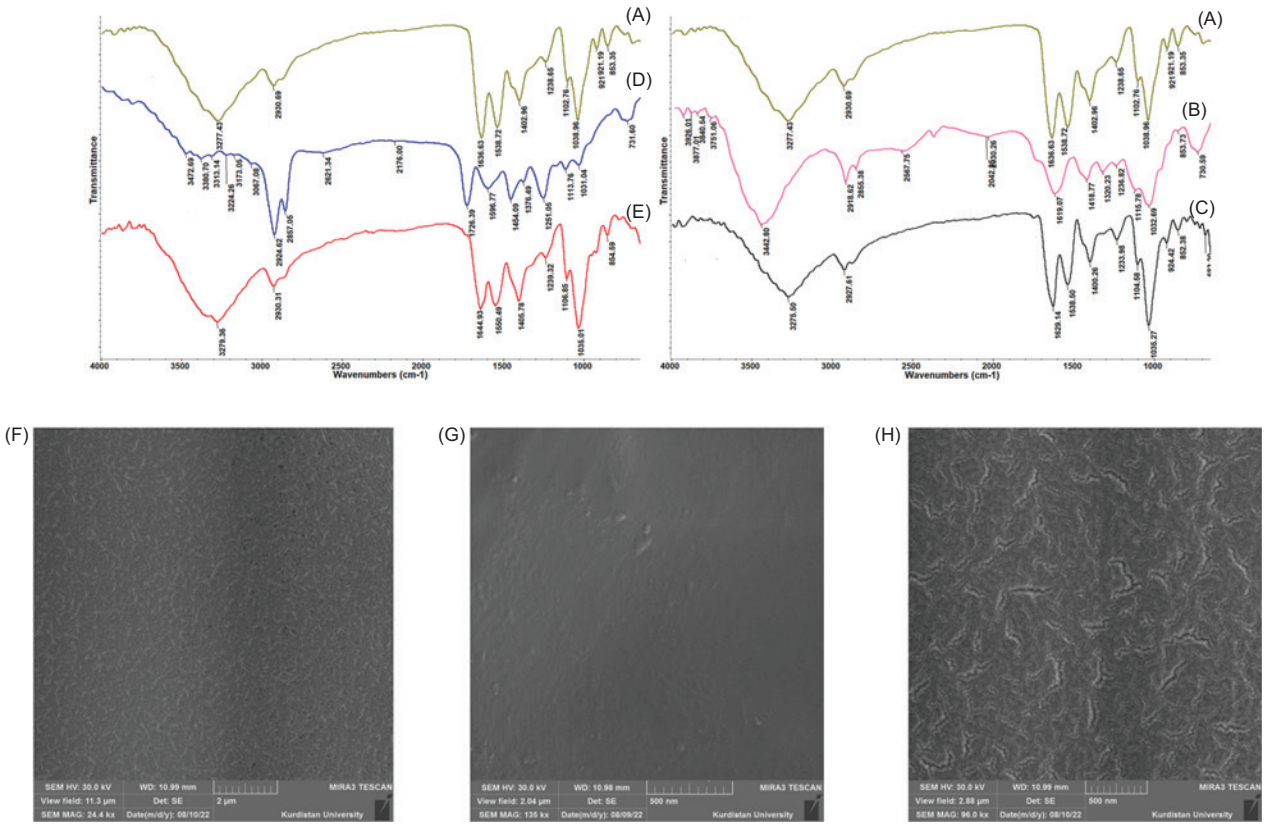

Figure 1. FTIR spectroscopy of SPI (A), JNPs (B), SPI- JNPs (C), CDs (D), SPI-CDs (E) and FESEM images of SPI (F), SPI-CDs (G), SPI- JNPs (H).

of the present study. Therefore, the proposed mechanistic interpretations should be considered preliminary, and additional analyses will be required in future work to confirm these assumptions more rigorously.

Mechanical properties

Different studies have indicated that nanomaterials effectively enhance the mechanical properties of SPI films (Huang *et al*., 2021). The incorporation of CDs and JNPs caused a decrease in EAB, an increase in TS, and an increase in the elastic modulus of SPI films (Table 1). These changes were concentration-dependent, although they were not always statistically significant. JNPs at the highest concentration (0.1%) showed the best performance, achieving the highest TS (15.2 ± 1.5 MPa) and elastic modulus (175.7 ± 2.5 MPa) among all samples ($p < 0.05$). This enhancement is likely attributable to the dual structure and favorable dispersion of JNPs within the protein matrix, which enable more efficient physical interactions and the formation of a percolating network. The simultaneous decrease in EAB and increase in TS provide insight into the reinforcement mechanism of the material. This observation suggests that weak physical interactions, such as van der Waals forces, hydrogen bonding, or physical entanglement, can enhance mechanical strength without inducing significant shifts in the characteristic vibrational frequencies of the main chemical bonds, as detected by FTIR. This physically crosslinked network significantly restricts the mobility and slippage of protein polymer chains under tensile stress. Notably, in the SPI-CD0.03%, SPI-JNPs0.03%, and SPI-JNPs0.05% films, no significant change was observed in the EAB properties compared with the SPI film ($p > 0.05$). Regarding TS, a significant enhancement ($p < 0.05$) for SPI-CDs was observed only at a 0.1% concentration (14.2 ± 2.4 MPa), while the TS at lower concentrations (0.03% and 0.05%) was not statistically different from the control ($p > 0.05$). In contrast, JNPs caused a significant increase in TS ($p < 0.05$) starting from a 0.05% concentration (12.2 ± 2.5 MPa). The observed mechanical response, characterized by increased strength and stiffness at the expense of ductility, is indicative of the classic strength–ductility trade-off. This phenomenon is commonly observed in polymer nanocomposites reinforced with rigid nanofillers, where the fillers act primarily through physical reinforcement and load transfer, inherently

Table 1. Mechanical characteristics including tensile strength (TS), elongation at break (EAB), modulus of elasticity and thickness of SPI, SPI-CDs, and SPI-JNP films.

Membrane	EAB (%)	TS (MPa)	Modulus of Elasticity (MPa)	Thickness (mm)
SPI	36.5 ± 0.5^{a}	9.6 ± 1.2^{C}	112.5 ± 0.5^{e}	0.75 ± 0.06^{a}
SPI- CD0.03%	35.9 ± 1.4^{a}	10.5 ± 1.5^{c}	118.8 ± 1.1^{d}	0.78 ± 0.08^{a}
SPI-CD0.05%	34.6 ± 0.9^{b}	11.1 ± 1.7^{bc}	123.6 ± 2.5^{d}	0.89 ± 0.02^{a}
SPI-CD0.1%	32.8 ± 0.5^{c}	14.2 ± 2.4^{ab}	155 ± 3^{b}	0.91 ± 0.03^{a}
SPI-JNP0.03%	36.19 ± 0.5^{a}	10.2 ± 1.1^{c}	113 ± 1^{e}	0.76 ± 0.05^{a}
SPI-JNP0.05%	35.2 ± 1.7^{a}	12.2 ± 2.5^{b}	141 ± 3^{c}	0.82 ± 0.08^{a}
SPI-JNP0.1%	31.4 ± 1.4^{c}	15.2 ± 1.5^{a}	175.7 ± 2.5^{a}	0.84 ± 0.04^{a}

Within each column, values with different letters are significantly different ($p < 0.05$).

restricting polymer chain mobility. This principle has been consistently reported in other bio-based nanocomposite systems. For instance, Oliveira *et al*. demonstrated that rigid starch nanocrystals reinforced mango kernel starch films through physical impingement, leading to a significant increase in tensile strength and elastic modulus, a trend perfectly aligned with our findings (Oliveira *et al*., 2018). The apparent contrast between this trend and some literature reports stems from the fundamentally different mechanisms imparted by various additives. For example, *Adilah et al.* (2018) observed that the EAB and TS of SPI films were enhanced with the incorporation of mango nanoparticles at a concentration of 3%. Cross-linking between amine groups of the protein and phenolic groups in the extract increased film hardness while reducing chain mobility and flexibility. These cross-links also restricted polymer chain mobility by reducing the plasticizing effect. This outcome was influenced by the diverse compounds present in the extracts, as some may enhance mechanical properties while others may reduce them (Adilah *et al*., 2018). Mirtalebi *et al.* (2019) reported that the addition of nanomaterials (MgO) to food packaging polymers at low concentrations and low loading capacities does not cause significant changes in mechanical properties, such as tensile stress at break. The different results reported in the literature highlight this variability. For example, Ghorbani *et al.* (2022) observed that incorporating CDs increased elongation at break and TS but decreased Young's modulus, showing that the mechanical response of nanocomposites is highly dependent on the specific type of nanomaterial, its surface properties, and its interfacial compatibility with the polymer matrix.

Although the thickness of SPI films (Table 1) showed an increasing trend with increasing CDs and JNPs concentrations, these differences were not statistically significant ($p > 0.05$). The SPI-CD0.1% film showed the highest thickness among all SPI-based films. A similar result was reported for SPI nanocomposite films prepared from silver nanoparticles and chitin nanowhiskers (Koshy *et al*., 2022).

UV-barrier analysis

UV radiation in the 200–400 nm range accelerates oxidation and causes off-flavors, browning, and nutrient loss in packaged food (Tripathi *et al*., 2024). The UV-barrier results revealed that the incorporation of CDs and JNPs significantly improved the UV-blocking performance of SPI films relative to the unfilled control (Figure 2). Within the 200–570 nm range, the barrier performance of CD- and JNP-loaded films followed a similar trend. All films, including the neat SPI film, completely blocked UV transmission in the 200–330 nm range (0% transmittance). Beyond 340 nm, the behavior of the films differed. While the transmittance of neat SPI increased significantly, reaching 12.0% at 360 nm and 30.2% at 400 nm, the SPI-CD and SPI-JNP films maintained exceptionally low transmittance values of only 0.7% at 360 nm and 1.5% and 1.0% at 400 nm, respectively, indicating the substantial contribution of these nanoparticles to the UV-blocking performance of the films. This corresponds to a 95.0% and 96.7% reduction in transmittance relative to the control at 400 nm, calculated using Eq. 6.

$$\text{Reduction in T\%} = [(T_{SPI} - T_{JNP/CD}) / T_{SPI}] \times 100 \quad \text{Eq. (6)}$$

Huang *et al.* (2021) reported that SPI films incorporated with mangosteen skin extract and ZnO nanoparticles were 90% effective in blocking UV radiation. The impact of CDs on the barrier properties of polyvinyl alcohol films revealed that the films had low light transmission below 900 nm. In a related study, Konwar *et al.* (2015) reported that chitosan films containing CDs permitted

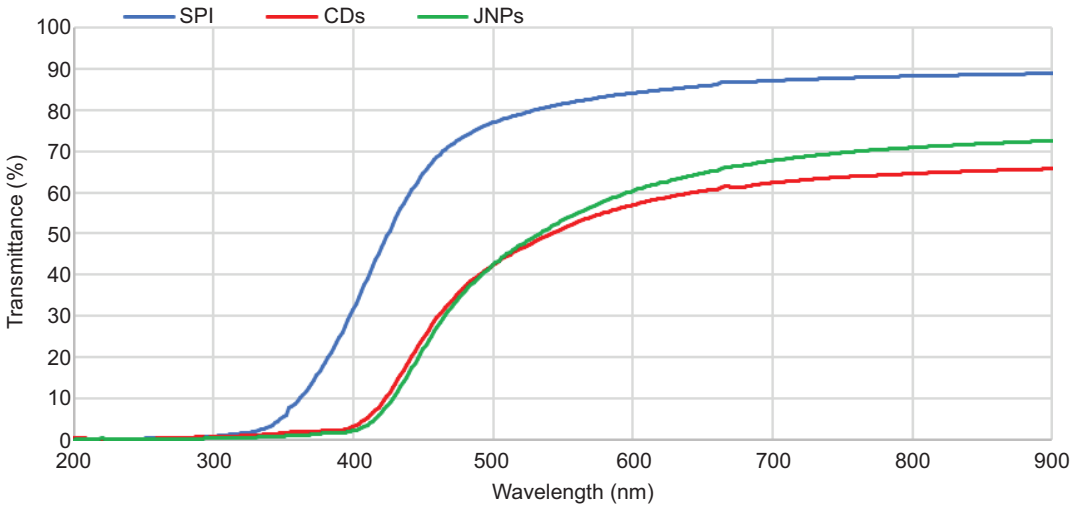

Figure 2. The transmission spectra of the SPI, SPI-CDs, and SPI- JNPs in the range of 200–900 nm.

only 20% light transmission in the 800–1000 nm range, indicating their effective barrier properties. Moreover, Yang *et al*. (2016) highlighted the ability of CD-embedded carboxymethyl cellulose films to photoconvert UV light into blue light, suggesting their potential for light-management applications.

Color properties

Table S1 and Figure S2 show the colorimetry and color specifications of the developed SPI films. With the addition of CDs, the L^* value of the films significantly decreased compared to that of the SPI film ($p < 0.05$). The greatest decrease was observed for SPI-CD0.1% (65.4 ± 0.8). The addition of JNPs also induced a general decreasing trend in the L^* value; however, for SPI-JNP0.05%, a slight numerical increase in the L^* value was observed. It is important to note that this increase was not statistically significant compared to the SPI film ($p > 0.05$). Regarding a^* values, the addition of both CDs and JNPs significantly increased the a^* values compared to the SPI film ($p < 0.05$) (except at 0.03%), and SPI-CD0.1% had the highest a^* value. Similarly, the addition of CDs and JNPs significantly increased the b^* value ($p < 0.05$). reported that, as the concentration of CDs increased from 1% to 5%, the color of gelatin/carrageenan-based films became darker, and the L^* value of the films decreased from 91.2 to 88.9. The a^* values decreased from 92.5 to 86.8, whereas the b^* values increased from 6.9 to 12.8. They reported that the influence of CDs on film color depends on both the CDs concentration and the color of the polymer matrix. The impact of turmeric-derived CDs on the color characteristics of pectin/gelatin films was also examined. By combining turmeric CDs and sulfur-doped CDs, the L^* value of the films decreased from 87.8 to 85.7 and 82.80, and the color of the films became yellowish-brown. The a^* values increased from –0.8 to 1.1 and 3.3, and the b^* values also increased from 17.7 to 27.5 and 29.4 (Ezati *et al*., 2022).

Release pattern

The migration of nanomaterials from food packaging is influenced by a number of factors, such as the concentration of nanomaterials, moisture levels, and the properties of the food product and packaging film. Research indicates that nanomaterials exhibit greater solubility and mobility in liquid and soft food matrices, such as apple juice and soft cheese ((Nwabor *et al*., 2020). Figure 3 shows the release behavior of JNPs and CDs from SPI films, influenced by the type of simulant and the solubility of the nanomaterials. The most polar simulant (10% ethanol) yielded the highest release of JNPs (40% at 0.1%) and the lowest release of CDs (9.29% at 0.1%) (Figure 3A). In contrast, the fatty-food simulant (95% ethanol) resulted in high release for both groups, with CDs at 0.1% showing the highest release (44.27%) (Figure 3C). In the oil-in-water emulsion food simulant (50% ethanol), 0.1% JNPs (34.35%) were released more rapidly than 0.1% CDs (32.06%) due to the amphiphilic nature of JNPs (Figure 3B). Although detailed kinetic modeling was not performed, the release behavior can be mechanistically interpreted based on diffusion and matrix relaxation phenomena. The amphiphilic character of JNPs may modulate their partitioning between food simulants of varying polarity, explaining the differential release profiles observed across the three simulant systems. The observed release pattern suggests

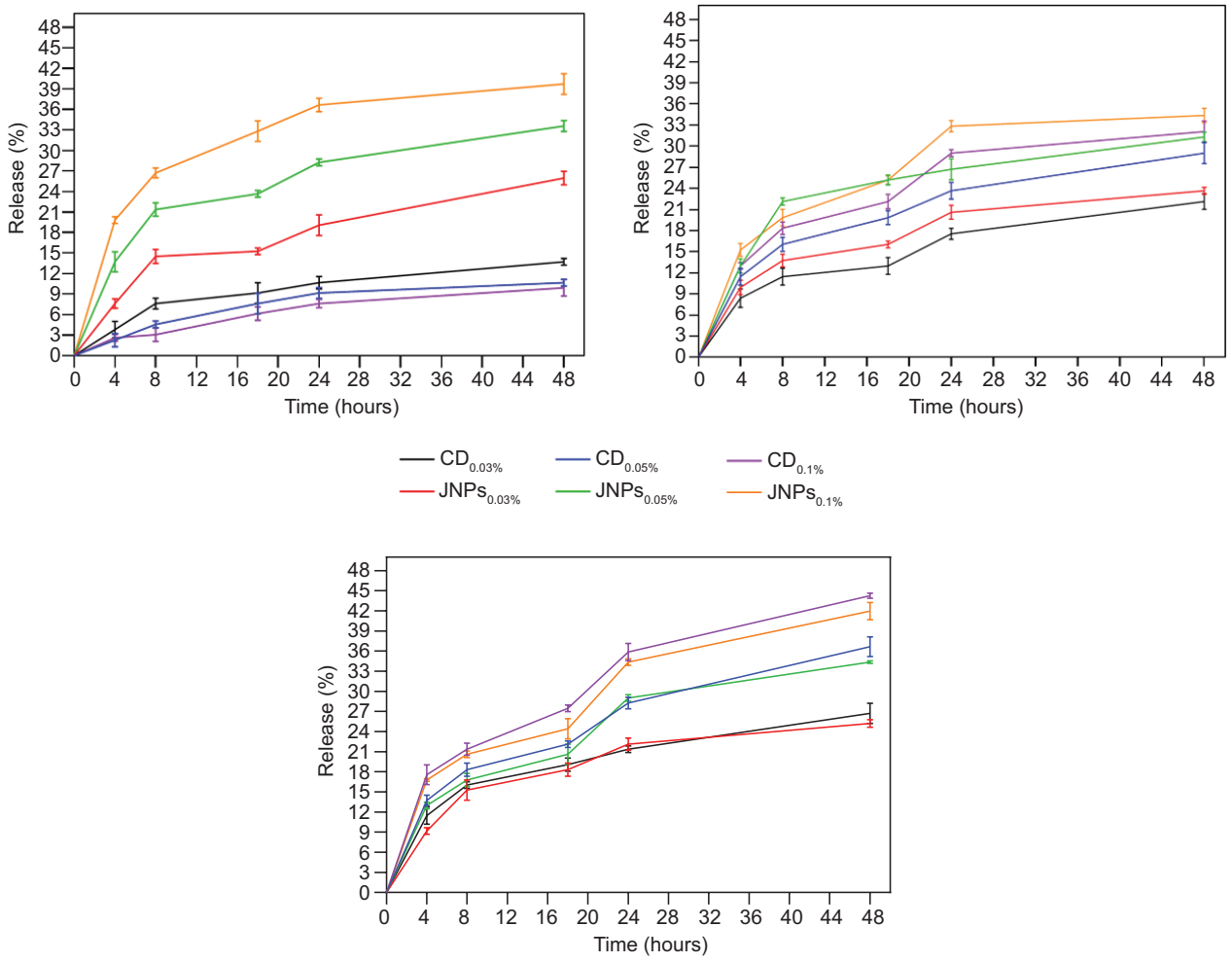

Figure 3. Release rate of the JNPs and CDs from the SPI films in various food simulant solutions. A: (10% ethanol), B: (50% ethanol), C: (95% ethanol).

a combination of Fickian diffusion and swelling-controlled transport, particularly in aqueous simulants. The hydrophilic nature of SPI films facilitates solvent penetration, leading to polymer relaxation and the formation of diffusion pathways for nanoparticle migration. This effect is more pronounced at higher JNPs concentrations and in polar media. However, the absence of formal kinetic modeling represents a limitation of the present study.

In our previous study, JNPs exhibited cytotoxicity only above a threshold concentration of 5 mg/mL. Crucially, the estimated maximum cumulative migration from the films is several orders of magnitude lower than the established cytotoxicity thresholds for these specific nanoparticles (5 mg/mL for JNPs and 1.5 mg/mL for CDs based on the MTT assay) (Razavi *et al.*, 2024), indicating a significant safety margin for food contact applications. It is important to note that no specific migration limit currently exists for nanoparticles under regulations such as EU 10/2011. To date, research on the release of CDs from food simulants remains limited. Ezati *et al.* (2022) investigated the release rate of hydrophilic CDs derived from *Enoki* mushrooms incorporated into gelatin/carrageenan films. CD release was significantly slower in 95% and 50% ethanol simulants than in 10% ethanol and pure water. Similarly, glucose- and nitrogen-derived CDs released from cellulose nanofiber films showed higher release in water than in ethanol, consistent with their hydrophilic nature.

From a regulatory perspective, the migration of NPs from food-contact materials remains an area of ongoing evaluation. Current frameworks, such as EU Regulation No. 10/2011, do not define specific migration limits for many nanostructured materials, including carbon-based NPs.

Although the estimated migration levels in this study are significantly lower than previously reported cytotoxicity thresholds, this alone does not constitute a comprehensive risk assessment. Therefore, the safety assessment presented here should be interpreted with caution, and further toxicological and regulatory studies are required before practical application.

Antioxidant activity

The antioxidant activities of SPI films incorporating 0.03, 0.05, and 0.1% concentrations of CDs and JNPs were evaluated using the DPPH radical-scavenging assay and FRAP methods. It should be noted that the dissolution-based extraction method used here measures the intrinsic antioxidant capacity of the film material and does not replicate the surface-contact kinetics expected under real packaging conditions. As illustrated in Figure 4A and B, the antioxidant effects exhibited a positive correlation with the concentrations of CDs and JNPs, with CDs indicating higher antioxidant capacity than JNPs. The unfilled SPI film exhibited approximately 5% DPPH radical-scavenging activity and a FRAP value of 7 μmol $FeSO_4$ equivalent. This is consistent with the known inherent antioxidant properties of SPI, attributed to naturally occurring polyphenols such as flavonoids and phenolic acids (Rani *et al*., 2021). The antioxidant activity of CDs depends on several factors, such as precursor type, surface functional groups, sp^2 carbon domain abundance, heteroatom doping, and structural defects. Their antioxidant effectiveness primarily arises from radical adduct formation at sp^2 sites, where a higher abundance of these domains enhances scavenging capacity. CDs with fewer sp^2 domains, however, rely predominantly on electron-transfer mechanisms (Zhao *et al*., 2022a). Additionally, hydrophobic surface groups on CDs may facilitate electron donation, further contributing to their antioxidant performance. Similarly, the antioxidant properties of JNPs can be attributed to their hydroxyl, carboxyl, and C–O functional groups, as confirmed by FTIR analysis (Razavi *et al*., 2024).

Antibacterial activity

Antimicrobial results showed that higher JNPs concentrations in the films led to larger inhibition zones (Figure 5A). In the agar disc diffusion test, the antibacterial effectiveness of nanomaterials is classified according to the inhibition zone diameter (ZOI) as follows: non-sensitive (<9 mm), sensitive (9–14 mm), very sensitive (14–19 mm), and extremely sensitive (>20 mm) (Ghorbani *et al*., 2022). Notably, in the agar disc diffusion assay, the largest ZOI against *L. monocytogenes* was achieved by the SPI-JNP film (26.7 mm, extremely sensitive), while the largest ZOI against *E. coli* was recorded for the SPI-CD film (23.15 mm, extremely sensitive). SPI films exhibited no antibacterial effect against either bacterium. A similar finding was reported in a previous study, where Razavi *et al*. (2024) noted that JNPs were more effective than CDs against *L. monocytogenes*. This difference may be attributed to the distinct cell wall structures of Gram-positive and Gram-negative bacteria (Molaei *et al*., 2025). negative bacteria have a complex cell wall structure characterized by double membranes and a thin peptidoglycan layer. In contrast, the thick peptidoglycan layer of Gram-positive bacteria offers less resistance to amphiphilic NPs such as JNPs, explaining their greater susceptibility (Ezati *et al*., 2022). Ma *et al*. (2023) revealed that Janus films incorporating silver nanoparticles/soybean polysaccharides/lotus leaf/beeswax exerted potent

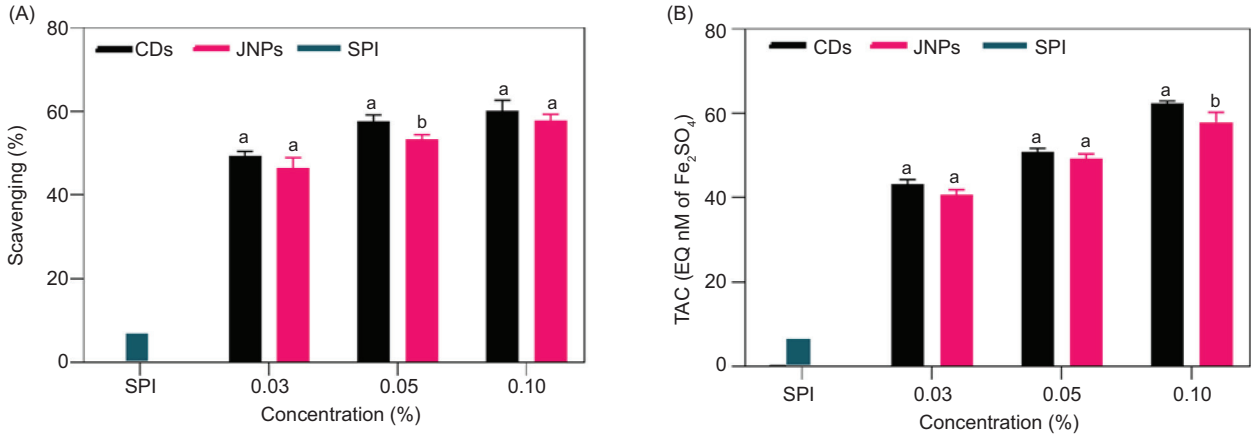

Figure 4. The antioxidant properties of SPI, SPI-CDs, and SPI-JNPs are illustrated through DPPH (A) and FRAP (B) assays. At each concentration level, values marked with different letters indicate a significant difference ($p < 0.05$).

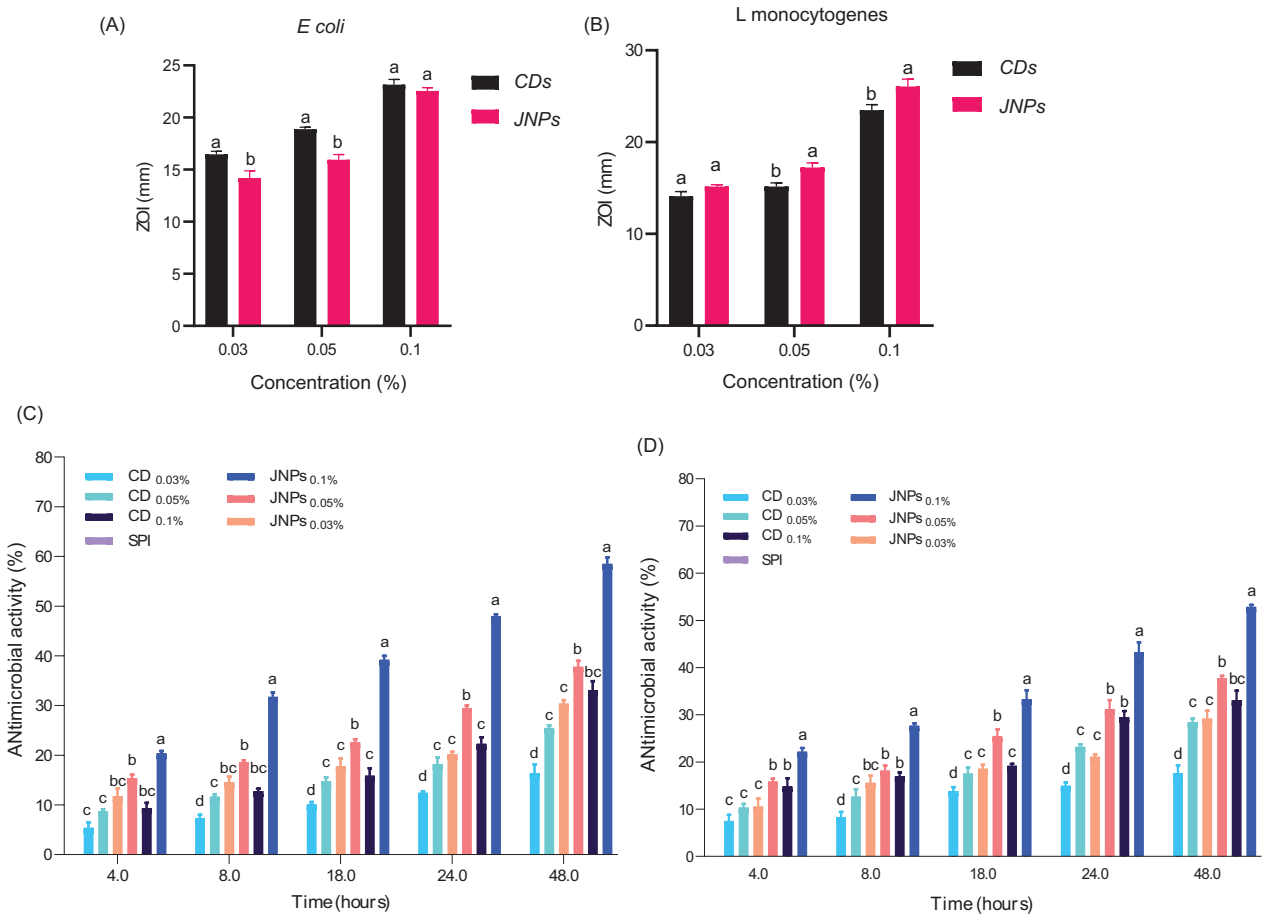

Figure 5. Effect of different concentrations of CDs and JNPs on *E. coli* and *L. monocytogenes* (A). Antimicrobial activity of SPI, SPI-CDs, and SPI-JNPs against *L. monocytogenes* (B) and *E. coli* (C) in TSB media. Different letters within each concentration and day indicate significant differences ($p < 0.05$).

bactericidal effects, eliminating 90% of both Gram-positive (*Staphylococcus aureus*) and Gram-negative (*E. coli*) populations.

Antibacterial efficacy in broth medium generally increased with increasing concentrations of CDs and JNPs in SPI films (Figure 5B,C). In this test, the SPI-JNP films exhibited the strongest antibacterial effects against both *L. monocytogenes* and *E. coli*. The superior performance of SPI-JNP films in broth may be attributed to the hydrophilic nature of the SPI matrix, which facilitates interaction with the aqueous TSB environment and promotes nanoparticle release. The antibacterial efficacy of these nanomaterials is influenced by multiple factors, including the physicochemical properties of CDs, microbial type, experimental method, and culture medium (Esmaeili Koutamehr *et al.*, 2023). SPI-CD films effectively prevented the growth of *E. coli* and *L. monocytogenes*, but *E. coli* was more sensitive to CDs than *L. monocytogenes*. Esmaeili Koutamehr *et al.* (2023) reported that Gram-negative bacteria (*Salmonella Typhimurium*) were more susceptible to sour whey-derived CDs than Gram-positive bacteria (*L. monocytogenes*) in the TSB medium. Jia *et al.* (2015), revealed that silver/chitosan Janus particles at 0.02 mg/mL effectively inhibited the growth of *E. coli*, *S. aureus*, *B. subtilis*, and *B. cinerea*. JNPs exhibit their antibacterial effect primarily through the physical disruption of bacterial cell structures. Upon exposure, JNPs adhere to the bacterial cell wall, disrupting its integrity and causing rupture. This breach allows JNPs to penetrate the cell and interfere with intracellular components, ultimately causing leakage of cellular contents and cell death (Razavi *et al.*, 2024). In contrast, CDs primarily act through chemical mechanisms such as oxidative stress induction (Molaei *et al.*, 2025). Thus, the key advantage of JNPs lies in their ability to physically disrupt bacterial membranes, a property facilitated by their amphiphilic Janus architecture.

Meat application

Microbial analysis

The influence of SPI, SPI-JNPs, and SPI-CDs films on TMBC and TPBC was examined (Figure 6A,B). In the control sample, TMBC and TPBC increased from 4.4 and 3.8 $\log_{10}$ CFU/g on day 0 to 9.5 and 8.4 $\log_{10}$ CFU/g on day 9, respectively. In the CDs and JNPs treatment groups, the same increasing trend was observed in bacterial populations at concentrations of 0.03% and 0.05%. In contrast, at the 0.1% level, a slow but steady increase in bacterial counts was observed. These results indicate that the SPI-CDs and SPI-JNPs films exhibit antimicrobial activity against meat microbiota in a concentration-dependent manner. Beef is considered spoiled and organoleptically unacceptable when TMBC and TPBC exceed 7 $\log_{10}$ CFU/g ((Mirmoeini *et al*., 2023).

On day 9, TMBC in samples treated with 0.1% SPI-CDs and SPI-JNPs films reached 5.4 and 5.1 $\log_{10}$ CFU/g, respectively. For TPBC, the bacterial population increased to 4.7 and 4.2 $\log_{10}$ CFU/g, respectively. Compared to the control sample on the same day, the reductions were as follows: for TMBC, 4.1 $\log_{10}$ CFU/g (SPI-CDs 0.1%) and 4.4 $\log_{10}$ CFU/g (SPI-JNPs 0.1%); for TPBC, 3.7 $\log_{10}$ CFU/g (SPI-CDs 0.1%) and 4.2 $\log_{10}$ CFU/g (SPI-JNPs 0.1%). However, statistical analysis revealed no significant difference between the efficacy of the 0.1% SPI-JNP and 0.1% SPI-CD films ($p > 0.05$). The TMBC of beef treated with films containing 0.05% CDs and JNPs reached 6.9 and 6.1 $\log_{10}$ CFU/g, respectively. In the 0.03% treatments, TMBC increased to 8.6 and 8.1 $\log_{10}$ CFU/g, respectively, indicating that these levels were insufficient to prevent the growth of microbial spoilage in the meat. In the control and SPI groups, TMBC increased to 7.8 and 8.1 $\log_{10}$ CFU/g, respectively, on day 6. The higher bacterial counts in the SPI film group are attributed to greater moisture absorption within the meat, which promotes microbial growth (Yong *et al*., 2023). These results indicate the efficacy of SPI-JNPs films, particularly at the 0.1% concentration, in extending the shelf life of minced meat by effectively suppressing microbial growth. The comparable antimicrobial activity of SPI-CD and SPI-JNP films at equal concentrations suggests that both nanomaterials confer strong antibacterial properties when incorporated into SPI matrices. Ma *et al*. (2023) reported a gradual increase in the total viable count of chicken and pork wrapped in JNPs films (constituted of soybean polysaccharides, lotus leaf, silver nanoparticles, and beeswax). Nevertheless, the wrapped samples showed pronounced microbial inhibition across all film concentrations, reflecting the strong antibacterial activity of Janus films during cold storage. These findings confirm the potential of such composite films to extend the shelf life of perishable meat products by controlling bacterial growth (Ma *et al*., 2023). SPI-based films incorporating CDs and JNPs showed greater inhibitory activity against TMBC than TPBC in meat samples. Several studies indicate that CDs have a stronger impact on TMBC than on TPBC (Ghorbani *et al*., 2024; Razavi *et al*., 2024). Psychrophilic microorganisms have special mechanisms that allow them to survive in cold environments. Such adaptations, including modifications in membrane composition, enzyme activity, and metabolic pathways, may enhance their tolerance to antimicrobial agents (Collins and Margesin, 2019).

pH

pH is among the most important indicators of meat freshness and quality, and its changes, in combination with other parameters, reflect the degree of spoilage. pH has a close relationship with the growth of microorganisms and food spoilage (Amiri *et al*., 2019). Figure 6C shows the pH changes in meat samples wrapped with SPI films containing 0.03%, 0.05%, and 0.1% CDs and JNPs. In the control group and the SPI film group without nanoparticles, pH increased from 5.9 ± 0.1 on day 0 to 7.1 ± 0.1 and 7.2 ± 0.1 on day 9 for the control and SPI groups, respectively, which were the highest values among all samples. This may be attributed to protease- or lipase-mediated hydrolysis reactions or the microbial degradation of amino acids (Amjadi *et al*., 2020). In general, minced meat with a pH exceeding 7.0 is considered unacceptable for consumption. The pH values of samples treated with 0.05% and 0.1% CDs and JNPs remained below 6.50 at the end of the 9-day storage period. The pH values recorded in the samples containing SPI-CDs and SPI-JNPs films at the same concentrations were not significantly different. In some cases, SPI-CDs exhibited a slightly lower pH, possibly due to the inherent acidity of the CDs (Razavi *et al*., 2024). Moreover, Fu *et al*. (2022) reported that fish meat wrapped in a chitosan film incorporated with CDs showed a lower pH after 10 days of storage compared to the control group.

TVB-N

Microbial proliferation generates metabolites such as organic acids, biogenic amines, volatile fatty acids, nitrogenous compounds, and sulfur compounds, creating color, odor, and flavor defects in foods (Ghorbani *et al*., 2024). TVB-N content was approximately 2.2 ± 0.3 mg/100 g in the meat sample on day 0 (Figure 6D). TVB-N increased progressively in all samples throughout storage, with the most pronounced rise observed in the control and unfilled SPI film groups. TVB-N concentrations in these samples on day 9 were 15.3 ± 0.7 mg/100 g and 14.8 ± 0.6 mg/100 g, respectively. Compared with the control, TVB-N levels in samples treated with 0.05% and 0.1% JNPs and CDs increased

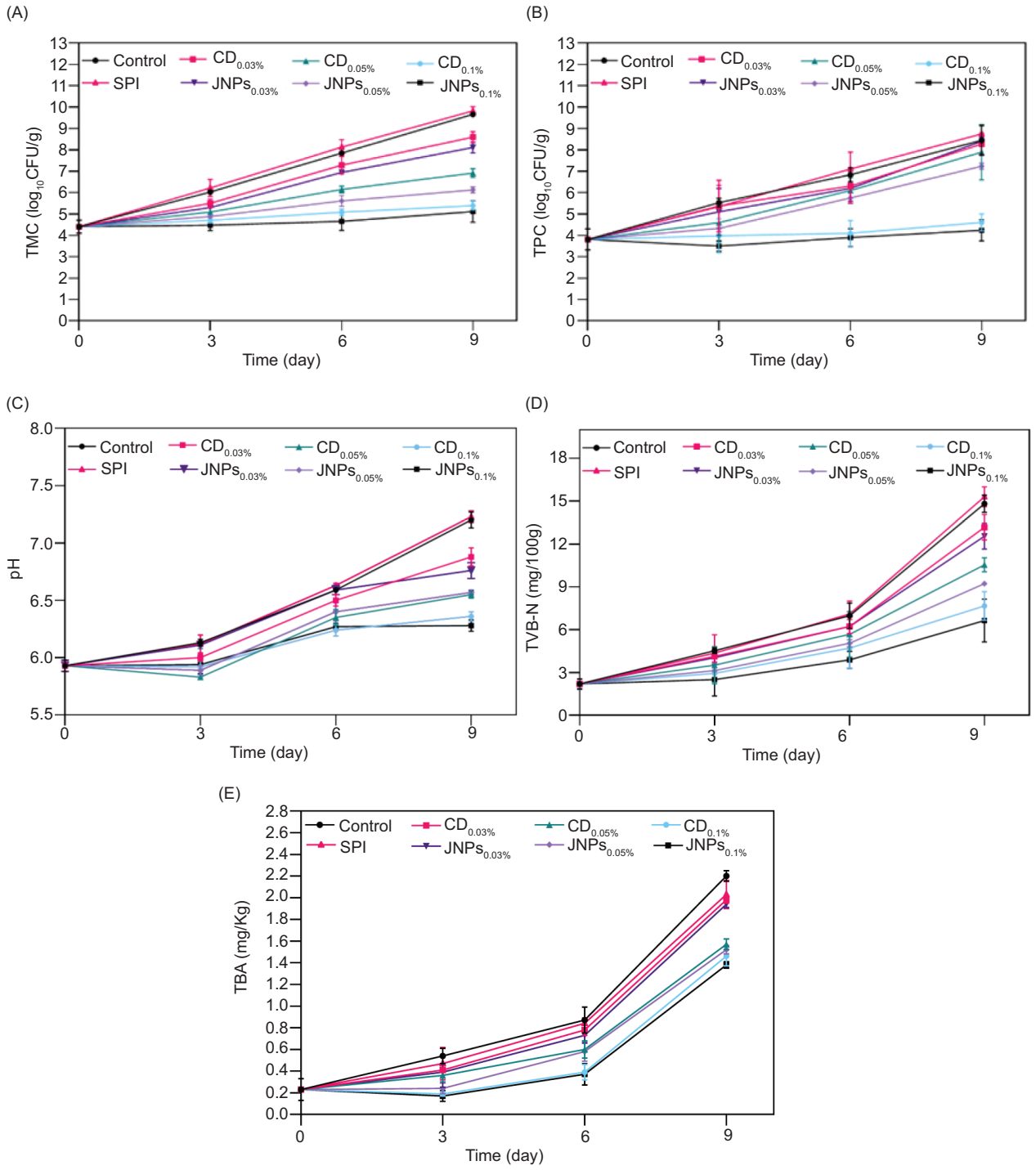

Figure 6. Bacteriological and chemical analyses of meat packaged with SPI films, SPI-CDs, and SPI-JNPs films (0.03%, 0.05%, and 0.1%) during storage at 7 °C. Microbial growth is represented by the total mesophilic bacteria count (A) and total psychrophilic bacteria count (B). Chemical analyses include pH (C), total volatile basic nitrogen (D), and thiobarbituric acid reactive substances (E).

more slowly, remaining below the spoilage threshold throughout storage. Although acceptable limits vary by regulatory authority, TVB-N values of 15–25 mg/100 g are generally considered indicative of spoilage (Mirmoeini *et al.*, 2023). The results indicate that the 0.05% and 0.1% concentrations of CDs and JNPs suppress biochemical activity and volatile compound formation, with the 0.1% level showing the greatest effect. No significant differences were observed between SPI-CDs and SPI-JNPs films at the same concentrations.

Razavi *et al*. (2024) reported that 0.05% CDs and JNPs significantly inhibited TVB-N formation ($p < 0.05$) in beef during storage, indicating concentration-dependent effects. In that study, treated samples maintained TVB-N values between 6.98 and 7.49 mg/100 g, below spoilage levels through day 9, attributed to the antimicrobial activity of the nanoparticles.

TBARS

The TBARS assay measures secondary lipid oxidation metabolites, of which MDA is the primary marker and an established indicator of oxidative deterioration (Fu *et al*., 2022). The meat initially presented a TBARS value of 0.2 mg MDA/kg (Figure 6E), reflecting freshness (Amjadi *et al*., 2020; Zhao *et al*., 2022a). Throughout storage, TBARS values increased in all samples, with the control reaching the highest value of 2.2 mg MDA/kg on day 9, which was significantly different from those of the other samples. For the SPI film without nanoparticles, the TBARS value was 2.0 mg MDA/kg on day 9, lower than that of the control samples, due to the antioxidant nature of SPI mentioned above. On day 9, TBARS values for SPI-CD films at 0.03%, 0.05%, and 0.1% were 2.0, 1.6, and 1.2 mg MDA/kg, respectively, while those for SPI-JNP films were 1.9, 1.5, and 1.0 mg MDA/kg, respectively, all of which were lower than the established TBARS limit (2 mg MDA/kg) (Amjadi *et al*., 2020). It should be noted that TBARS values decreased with increasing nanoparticle concentration. The TBARS values of SPI-JNPs were lower than those of SPI-CDs films at the same concentrations, although the difference was not significant. Similarly, Semsari *et al*. (2024) reported reduced TBARS values in beef treated with lemon peel-derived CDs at 5 and 10 mg/mL. Although TBARS values increased in both control and treated samples during storage, the rise was markedly slower in CD-treated meat, indicating inhibition of free radical activity and lipid oxidation. In previous research, TBARS values of fried meatballs containing CDs decreased significantly after storage at 4 °C (Zhao *et al*., 2022b), which is consistent with the findings of the present study.

Color changes

During storage, a^* (redness), L^* (lightness), and b^* (yellowness) values of all samples showed a decreasing trend (Figure S3). The reduction in a^* and L^* values is attributed to the yellow coloration imparted by JNPs and CDs, which affects the lightness of the meat surface (Semsari *et al*., 2024). The greatest reduction in L^* was observed in SPI-CD0.1%, and the greatest reduction in a^* was observed in the control sample. The SPI-JNP sample, however, had the highest b^* value. The increases in a^* and b^* observed throughout the storage period are due to the oxidation of oxymyoglobin to metmyoglobin (Sayadi *et al*., 2022). Previous studies have confirmed that the incorporation of colored CDs in meat packaging reduces L^* and b^* values and increases a^* values, which is most likely due to the bleaching and darkening effects of meat myoglobin (Sul *et al*., 2023; Ghorbani *et al*., 2024). The use of low NPs concentrations effectively minimized color changes, highlighting their suitability for food packaging applications requiring color preservation. This observation supports the widely reported finding that optimal low levels of nanoparticles can help maintain high-quality food and prevent undesired changes commonly associated with high concentrations (Wasilewska *et al*., 2023).

Sensory analysis

Figure 7 presents the sensory evaluation results (*color*, *aroma*, and *overall acceptability*) of meat wrapped with SPI films containing 0.03%, 0.05%, and 0.1% CDs and JNPs. SPI-JNP films at 0.03% and 0.05% received higher color scores than the other samples after 9 days of storage. With respect to the overall acceptability of the control and SPI film samples, a noticeable decrease was observed during the 9-day storage period. Among the CD- and JNP-incorporated samples, SPI-CD0.05% and SPI-JNP0.1% received the highest odor and overall acceptability scores, respectively, likely due to the mild smoky aroma contributed by CDs. The use of CDs incorporated bacterial cellulose films for minced meat preservation led to better sensory scores for aroma and overall acceptability compared with the control samples (Ghorbani *et al*., 2024).

PCA was performed to evaluate the effects of CDs and JNPs on meat quality parameters (Figure 8). The first two principal components together explained 95% of the total variance. PC1 primarily represented spoilage and oxidation metrics (such as pH, TVB-N, TBARS, and microbial counts), while PC2 was strongly associated with sensory quality attributes (color, odor, and overall acceptability). An inverse relationship was observed between the variables associated with PC1 (spoilage indicators) and PC2 (sensory attributes), indicating that increased spoilage corresponded with diminished sensory quality (Figure 8A). This pattern reflects the expected trade-off between spoilage progression and sensory quality deterioration in packaged meat. Specifically, concentrations of nanoparticles that effectively enhanced sensory attributes may have exhibited less pronounced effects on certain chemical or microbial parameters, or vice versa. The score and loading plots (Figure 8B,C) indicated that SPI-JNP0.1% and SPI-CD0.1% films provided optimal chemical and microbial preservation in packaged meat samples. The high cumulative variance (95%) captured by the two components indicates strong intercorrelation among the measured quality parameters. This suggests

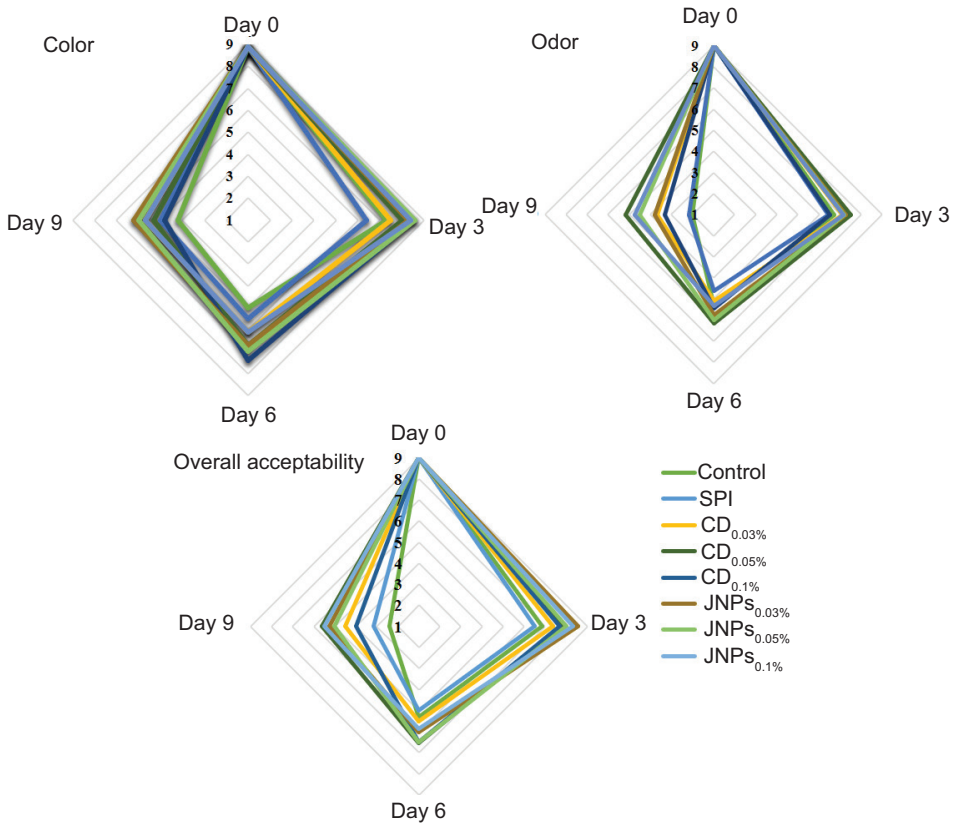

Figure 7. Sensorial properties of meat packaged with SPI films, SPI-CDs, and SPI-JNPs films (0.03%, 0.05%, and 0.1%) during storage at 7 °C.

that the preservative effects of CDs and JNPs are systematic and can be modulated through concentration optimization. These findings provide a basis for optimizing nanoparticle concentration in SPI-based packaging to simultaneously improve the microbial, chemical, and sensory quality of meat products.

Conclusion

The incorporation of JNPs into SPI films markedly enhances their mechanical, optical, and bioactive properties, thereby facilitating their use as effective active packaging materials. JNPs showed higher release in aqueous environments, which promoted antioxidant and antimicrobial activities. In addition, the incorporation of JNPs did not compromise the structural integrity of the films; rather, it enhanced their mechanical strength and UV-blocking capabilities. When applied to minced meat, the nanocomposite films reduced microbial counts by up to 4.7 $\log_{10}$ CFU/g and delayed the formation of chemical spoilage indicators, such as TVB-N and TBA. Sensory attributes also remained within acceptable ranges throughout the 9-day cold storage period. Limitations of this study include the absence of an in vivo safety assessment. These findings advance the understanding of multifunctional protein-based film design using Janus nanotechnology and support the development of sustainable active packaging for perishable foods. Future studies should address remaining challenges, including long-term stability, in vivo safety assessment for regulatory approval, and cost-effective scale-up. Evaluating the performance of alternative plant-based proteins, such as pea and rice protein, in diverse food matrices, including cheese, fresh-cut fruits, and bread, is also warranted.

Mandatory Disclosure on Use of Artificial Intelligence

The authors used Paperpal to improve the language and clarity of the text, and subsequently performed their own review and editing.

Author Contributions

R.R.: Investigation and writing–original draft. M.M.: Conceptualization, Formal analysis, and Writing – review & editing. H.T.: Supervision and Visualization.

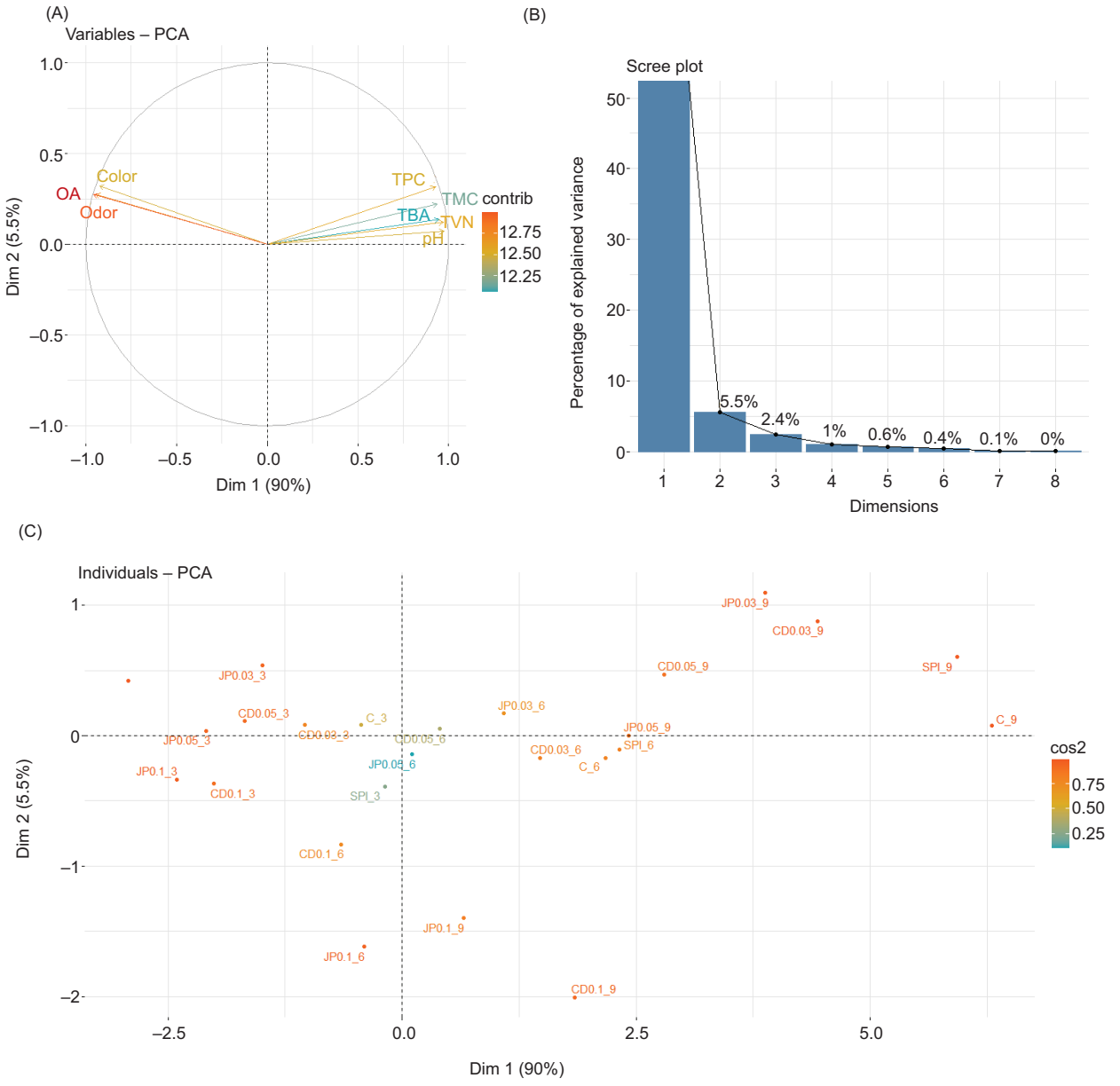

Figure 8. Principal component analysis of samples collected at four separate time intervals. (A) Vector depiction of the assessed parameters, (B) the contribution of the samples to variations in the first two principal components, and (C) the arrangement of samples according to the first two principal components. Total mesophilic bacteria count (TMC); total psychrophilic bacteria count (TPC); total volatile basic nitrogen (TVB-N); thiobarbituric acid (TBA); and overall acceptability (OA). Hydrophobic carbon dots (CDs) and Janus particles (JNPs) were used at concentrations of 0.03%, 0.05%, and 0.1%.

R.M.: Conceptualization, Methodology, Formal analysis, and Writing – review & editing.

Conflicts of Interest

The authors have declared that there is no conflict of interest.

Funding

This work is based on research funded by the Iran National Science Foundation (INSF) under project No. 4026654. We are also grateful for the financial assistance provided by the Faculty of Veterinary Medicine at Urmia University, Iran.

References

Adilah, Z. A. M., Jamilah, B., & Hanani, Z. A. N. (2018). Functional and antioxidant properties of protein-based films incorporated with mango kernel extract for active packaging. Food Hydrocolloids, 74, 207–218. https://doi.org/10.1016/j.foodhyd.2017.08.017

Ahmed, M. W., Haque, M. A., Mohibbullah, M., Khan, M. S. I., Islam, M. A., Mondal, M. H. T., & Ahmmed, R. (2022). A review on active packaging for quality and safety of foods: Current trends, applications, prospects and challenges. Food Packaging and Shelf Life, 33, 100913. https://doi.org/10.1016/j.fpsl.2022.100913

Akrami, S., Saki, M., Marashi Hossaeini, S. M., Sabahi, S., & Noori, S. M. A. (2023). Application of soy protein-based films and coatings on the shelf life of food products: A mini-review of recent publications with emphasis on nanotechnology. *Journal of* Food Measurement and Characterization, 17(2), 1393–1401. https://doi.org/10.1007/s11694-022-01708-4

Alizadeh, N., Moradi, M., Molaei, R., & Razavi, R. (2026). Bacterial nanocellulose films functionalized with Janus nanoparticles: Preparation and application in chicken meat preservation and safety. Scientific Reports, 7, 1–56. https://doi.org/10.1038/s41598-026-39029-x

Amiri, E., Aminzare, M., Azar, H. H., & Mehrasbi, M. R. (2019). Combined antioxidant and sensory effects of corn starch films with nanoemulsion of *Zataria multiflora* essential oil fortified with cinnamaldehyde on fresh ground beef patties. Meat Science, 153, 66–74. https://doi.org/10.1016/j.meatsci.2019.03.004

Amjadi, S., Nazari, M., Alizadeh, S. A., & Hamishehkar, H. (2020). Multifunctional betanin nanoliposomes-incorporated gelatin/chitosan nanofiber/ZnO nanoparticles nanocomposite film for fresh beef preservation. Meat Science, 167, 108161. https://doi.org/10.1016/j.meatsci.2020.108161

ASTM. (2012). *Designation D882-12: Standard test method for tensile properties of thin plastic sheeting.* Annual Book of ASTM Standards. American Society for Testing and Materials, Philadelphia.

Collins, T., & Margesin, R. (2019). Psychrophilic lifestyles: Mechanisms of adaptation and biotechnological tools. Applied Microbiology and Biotechnology, 103(7), 2857–2871. https://doi.org/10.1007/s00253-019-09659-5

Divsalar, E., Moradi, M., Tajik, H., Molaei, R., Conte, A., & Del Nobile, M. A. (2025). Improving the shelf life of fresh pasta filata cheese using lactobacilli postbiotics and carbon dots. Quality Assurance and Safety of Crops and Foods, 17(2), 106–123. https://doi.org/10.15586/qas.v17i2.1530

Esmaeili Koutamehr, M., Moradi, M., Tajik, H., Molaei, R., Khakbaz Heshmati, M., & Alizadeh, A. (2023). Sour whey-derived carbon dots: Synthesis, characterization, antioxidant activity, and antimicrobial performance against foodborne pathogens. LWT – Food Science and Technology, 184, 114978. https://doi.org/10.1016/j.lwt.2023.114978

Ezati, P., & Rhim, J.-W. (2021). Fabrication of quercetin-loaded biopolymer films as functional packaging materials. ACS Applied Polymer Materials, 3(4), 2131–2137. https://doi.org/10.1021/acsapm.1c00177

Ezati, P., Rhim, J.-W., Molaei, R., Priyadarshi, R., Roy, S., Min, S., Kim, Y. H., Lee, S. G., & Han, S. (2022). Preparation and characterization of B-, S-, and N-doped glucose carbon dots: Antibacterial, antifungal, and antioxidant activity. Sustainable Materials and Technologies, 32, 397. https://doi.org/10.1016/j.susmat.2022.e00397

Ezati, P., Roy, S., & Rhim, J.-W. (2022). Pectin/gelatin-based bioactive composite films reinforced with sulfur-functionalized carbon dots. Colloids and Surfaces A: Physicochemical and Engineering Aspects, 636, 128123. https://doi.org/10.1016/j.colsurfa.2021.128123

Fan, S., Yang, Q., Zhu, C., Li, X., Richel, A., Fauconnier, M., Fang, F., Zhang, D., & Hou, C. (2025). Zein/chitosan Janus film incorporated with tannic acid and cinnamon essential oil co-loaded Pickering emulsion for sustained controlled release and pork preservation. International Journal of Biological Macromolecules, 286, 138429. https://doi.org/10.1016/j.ijbiomac.2024.138429

Fu, B., Liu, Q., Liu, M., Chen, X., Lin, H., Zheng, Z., Zhu, J., Dai, C., Dong, X., & Yang, D.-P. (2022). Carbon dots enhanced gelatin/chitosan bio-nanocomposite packaging film for perishable foods. Chinese Chemical Letters, 33(10), 4577–4582. https://doi.org/10.1016/j.cclet.2022.03.048

Ghorbani, M., Moradi, M., Tajik, H., Molaei, R., & Alizadeh, A. (2024). Carbon dots embedded bacterial cellulose membrane as active packaging: Toxicity, in vitro release, and application in minced beef packaging. Food Chemistry, 433, 137311. https://doi.org/10.1016/j.foodchem.2023.137311

Ghorbani, M., Tajik, H., Moradi, M., Molaei, R., & Alizadeh, A. (2022). One-pot microbial approach to synthesize carbon dots from baker's yeast-derived compounds for the preparation of antimicrobial membrane. Journal of Environmental Chemical Engineering, 10(3), 107525. https://doi.org/10.1016/j.jece.2022.107525

Guerrero, P., Garrido, T., Leceta, I., & de la Caba, K. (2013). Films based on proteins and polysaccharides: Preparation and physical–chemical characterization. European Polymer Journal, 49(11), 3713–3721. https://doi.org/10.1016/j.eurpolymj.2013.08.014

Hadavifar, S., Abedi-Firoozjah, R., Bahramian, B., Jafari, N., Sadeghi, S. M., Majnouni, S., Ebrahimi, B., Ehsani, A., & Tavassoli, M. (2025). Multifunctional performance of chitosan/soy protein isolation-based films impregnated carbon dots/anthocyanin derived from purple hull pistachio for tracking and extending the shelf life of fish. Food Hydrocolloids, 159, 110678. https://doi.org/10.1016/j.foodhyd.2024.110678

Hosseiniyeh, N., Mohtarami, F., Almasi, H., & Azizi, S. (2024). Soy protein isolate film activated by black seed oil nanoemulsion as a novel packaging for shelf-life extension of bulk bread. Food Science & Nutrition, 12(3), 1706–1723. https://doi.org/10.1002/fsn3.3864

Hu, J., Li, D., Huai, Q., Geng, M., Sun, Z., Wang, M., Wang, S., Li, Y., & Zheng, H. (2023). Development and evaluation of soybean protein isolate–based antibacterial nanocomposite films containing nano-TiO2. Industrial Crops and Products, 197, 116620. https://doi.org/10.1016/j.indcrop.2023.116620

Huang, X., Zhou, X., Dai, Q., & Qin, Z. (2021). Antibacterial, antioxidation, UV-blocking, and biodegradable soy protein isolate food packaging film with Mangosteen peel extract and ZnO nanoparticles. Nanomaterials, 11(12). https://doi.org/10.3390/nano11123337

Jia, R., Jiang, H., Jin, M., Wang, X., & Huang, J. (2015). Silver/chitosan-based Janus particles: Synthesis, characterization, and assessment of antimicrobial activity in vivo and vitro. Food Research International, 78, 433–441. https://doi.org/10.1016/j.foodres.2015.08.035

Konwar, A., Gogoi, N., Majumdar, G., & Chowdhury, D. (2015). Green chitosan–carbon dots nanocomposite hydrogel film with superior properties. Carbohydrate Polymers, 115, 238–245. https://doi.org/10.1016/j.carbpol.2014.08.021

Koshy, R. R., Reghunadhan, A., Mary, S. K., Sadanandan, S., Jose, S., Thomas, S., & Pothen, L. A. (2022). AgNP anchored carbon dots and chitin nanowhisker embedded soy protein isolate films with freshness preservation for active packaging. Food Packaging and Shelf Life, 33, 100876. https://doi.org/10.1016/j.fpsl.2022.100876

Kumar, L., & Gaikwad, K. K. (2023). Carbon dots for food packaging applications. Sustainable Food Technology, 1(2), 185–199. https://doi.org/10.1039/D2FB00020B

Li, W., Li, X., Wang, Q., Pan, Y., Wang, T., Wang, H., Song, R., & Deng, H. (2014). Antibacterial activity of nanofibrous mats coated with lysozyme-layered silicate composites via electrospraying. Carbohydrate Polymers, 99, 218–225. https://doi.org/10.1016/j.carbpol.2013.07.055

Lin, F., Wang, Z., & Wu, F.-G. (2022). Carbon dots for killing microorganisms: An update since 2019. Pharmaceuticals, 15(10). https://doi.org/10.3390/ph15101236

Liu, Z., McClements, D. J., Shi, A., Zhi, L., Tian, Y., Jiao, B., Liu, H., & Wang, Q. (2022). Janus particles: A review of their applications in food and medicine. Critical Reviews in Food Science and Nutrition, 6, 1–12. https://doi.org/10.1080/10408398.2022.2067831

Ma, Z., Xing, Z., Zhao, Y., Zhang, H., Xin, Q., Liu, J., Qin, M., Ding, C., & Li, J. (2023). Lotus leaf inspired sustainable and multifunctional Janus film for food packaging. Chemical Engineering Journal, 457, 141279. https://doi.org/10.1016/j.cej.2023.141279

Madannejad, R., Shoaie, N., Jahanpeyma, F., Darvishi, M. H., Azimzadeh, M., & Javadi, H. (2019). Toxicity of carbon-based nanomaterials: Reviewing recent reports in medical and biological systems. Chemico-Biological Interactions, 307, 206–222. https://doi.org/10.1016/j.cbi.2019.04.036

Meerasri, J., Sukatta, U., Rugthaworn, P., Klinsukhon, K., Khacharat, L., Sakayaroj, S., Chollakup, R., & Sothornvit, R. (2024). Synergistic effects of thyme and oregano essential oil combinations for enhanced functional properties of sericin/pectin film. International Journal of Biological Macromolecules, 263, 130288. https://doi.org/10.1016/j.ijbiomac.2024.130288

Mirmoeini, S. S., Moradi, M., Tajik, H., Almasi, H., & Gama, F. M. (2023). Cellulose/Salep-based intelligent aerogel with red grape anthocyanins: Preparation, characterization, and application in beef. Food Chemistry, 425, 136493. https://doi.org/10.1016/j.foodchem.2023.136493

Mirtalebi, S. S., Almasi, H., & Alizadeh Khaledabad, M. (2019). Physical, morphological, antimicrobial, and release properties of novel MgO-bacterial cellulose nanohybrids prepared by in-situ and ex-situ methods. International Journal of Biological Macromolecules, 128, 848–857. https://doi.org/10.1016/j.ijbiomac.2019.02.007

Molaei, R., Razavi, R., Omer, A. K., Javid, A. L., Ezati, P., Nikfarjam, N., Lim, L.-T., & Moradi, M. (2025). Hydrophobic carbon dots: An overview of the synthesis, purification, cytotoxicity, and potential applications in food safety and analytical chemistry. Quality Assurance and Safety of Crops & Foods, 17(2), 136–164. https://doi.org/10.15586/qas.v17i2.1532

Mostafa, H., Airouyuwaa, J. O., Hamed, F., Wang, Y., & Maqsood, S. (2023). Structural, mechanical, antioxidant, and antibacterial properties of soy protein isolate (SPI)-based edible food packaging films as influenced by nanocellulose (NC) and green extracted phenolic compounds from date palm leaves. Food Packaging and Shelf Life, 38, 101124. https://doi.org/10.1016/j.fpsl.2023.101124

Nikfarjam, N., Razavi, R., Moradi, M., & Molaei, R. (2025). Green synthesis of carbon dots from onion juice and ex-situ embedding for antimicrobial/ultraviolet protective nanocellulose films. Food Safety and Packaging, 1(1), 24–32. https://doi.org/10.30466/fsp.2025.56060.1006

Nwabor, O. F., Singh, S., Paosen, S., Vongkamjan, K., & Voravuthikunchai, S. P. (2020). Enhancement of food shelf life with polyvinyl alcohol-chitosan nanocomposite films from bioactive *Eucalyptus* leaf extracts. Food Bioscience, 36, 100609. https://doi.org/10.1016/j.fbio.2020.100609

Oliveira, A. V., da Silva, A. P. M., Barros, M. O., de Sá M. Souza Filho, M., Rosa, M. F., & Azeredo, H. M. C. (2018). Nanocomposite films from mango kernel or corn starch with starch nanocrystals. Starch - Stärke, 70(11–12), 1800028. https://doi.org/10.1002/star.201800028

Rani, P., Yu, X., Liu, H., Li, K., He, Y., Tian, H., & Kumar, R. (2021). Material, antibacterial, and anticancer properties of natural polyphenols incorporated soy protein isolate: A review. European Polymer Journal, 152, 110494. https://doi.org/10.1016/j.eurpolymj.2021.110494

Rani, S., Kumar, K. D., Mandal, S., & Kumar, R. (2020). Functionalized carbon dot nanoparticles reinforced soy protein isolate biopolymeric film. Journal of Polymer Research, 27(10), 1–10. https://doi.org/10.1007/s10965-020-02276-1

Razavi, R., Molaei, R., Moradi, M., Tajik, H., Ezati, P., & Yordshahi, A. S. (2020). Biosynthesis of metallic nanoparticles using mulberry fruit (*Morus alba* L.) extract for the preparation of antimicrobial nanocellulose film. Applied Nanoscience, 10(2), 465–476. https://doi.org/10.1007/s13204-019-01137-8

Razavi, R., Tajik, H., Molaei, R., McClements, D. J., & Moradi, M. (2024). Janus nanoparticles synthesized from hydrophobic carbon dots and carboxymethyl cellulose: Novel antimicrobial additives for fresh food applications. Food Bioscience, 62, 105171. https://doi.org/10.1016/j.fbio.2024.105171

Roila, R., Sordini, B., Esposto, S., Ranucci, D., Primavilla, S., Valiani, A., Taticchi, A., Branciari, R., & Servili, M. (2022). Effect of the application of a green preservative strategy on minced meat products: Antimicrobial efficacy of olive mill wastewater polyphenolic extract in improving beef burger shelf-life. Foods, 11(16). https://doi.org/10.3390/foods11162447

Roy, S., Ezati, P., & Rhim, J.-W. (2021). Gelatin/carrageenan-based functional films with carbon dots from enoki mushroom for active food packaging applications. ACS Applied Polymer Materials, 3(12), 6437–6445. https://doi.org/10.1021/acsapm.1c01175

Sattariazar, S., Arsalani, N., & Nejad Ebrahimi, S. (2023). Biological assessment of synthesized carbon dots from polyphenol enriched extract of pomegranate peel, incorporated with *Mentha piperita* essential oil. Materials Chemistry and Physics, 294, 126981. https://doi.org/10.1016/j.matchemphys.2022.126981

Sayadi, M., Mojaddar Langroodi, A., Amiri, S., & Radi, M. (2022). Effect of nanocomposite alginate-based film incorporated with cumin essential oil and TiO2 nanoparticles on chemical, microbial, and sensory properties of fresh meat/beef. Food Science & Nutrition, 10(5), 1401–1413. https://doi.org/10.1002/fsn3.2724

Semsari, E., Tajik, H., Molaei, R., & Moradi, M. (2024). Innovative aerosol technology using lemon peel-derived carbon dots for improving shelf life of beef. Applied Food Research, 4, 100499. https://doi.org/10.1016/j.afres.2024.100499

Shafipour Yordshahi, A., Moradi, M., Tajik, H., & Molaei, R. (2020). Design and preparation of antimicrobial meat wrapping nanopaper with bacterial cellulose and postbiotics of lactic acid bacteria. International Journal of Food Microbiology, 321, 108561. https://doi.org/10.1016/j.ijfoodmicro.2020.108561

Shang, W., Ye, M., Cai, T., Zhao, L., Zhang, Y., Liu, D., & Liu, S. (2018). Tuning of the hydrophilicity and hydrophobicity of nitrogen doped carbon dots: A facile approach towards high efficient lubricant nanoadditives. Journal of Molecular Liquids, 266, 65–74. https://doi.org/10.1016/j.molliq.2018.06.042

Sul, Y., Ezati, P., & Rhim, J.-W. (2023). Preparation of chitosan/gelatin-based functional films integrated with carbon dots from banana peel for active packaging application. International Journal of Biological Macromolecules, 246, 125600. https://doi.org/10.1016/j.ijbiomac.2023.125600

Tripathi, S., Kumar, L., Deshmukh, R. K., & Gaikwad, K. K. (2024). Ultraviolet blocking films for food packaging applications. Food and Bioprocess Technology, 17(6), 1563–1582. https://doi.org/10.1007/s11947-023-03221-y

Wang, Z., Chen, Y., Zhang, N., Zhang, R. X., He, R., Ju, X., & Mamadalieva, N. Z. (2023). Plant protein nanogel–based patchy Janus particles with tunable anisotropy for perishable food preservation. Food Frontiers, 4(2), 795–806. https://doi.org/10.1002/fft2.219

Wasilewska, A., Bielicka, M., Klekotka, U., & Kalska-Szostko, B. (2023). Nanoparticle applications in food – A review. Food & Function, 14(6), 2544–2567. https://doi.org/10.1039/D2FO02180C

Xue, J., Ma, C., Yang, S., Guo, S., Yin, X., Fan, J., Li, X., Wang, M., & Teng, G. (2024). Janus hydrogel loaded with a CO2-generating chemical reaction system: Construction, characterization, and application in fruit and vegetable preservation. Food Chemistry, 458, 140271. https://doi.org/10.1016/j.foodchem.2024.140271

Yang, J., Zhang, X., Ma, Y.-H., Gao, G., Chen, X., Jia, H.-R., Li, Y.-H., Chen, Z., & Wu, F.-G. (2016). Carbon dot-based platform for simultaneous bacterial distinguishment and antibacterial applications. ACS Applied Materials & Interfaces, 8(47), 32170–32181. https://doi.org/10.1021/acsami.6b10398

Yavari Maroufi, L., Shahabi, N., Fallah, A. A., Mahmoudi, E., Al-Musawi, M. H., & Ghorbani, M. (2023). Soy protein isolate/kappa-carrageenan/cellulose nanofibrils composite film incorporated with zenian essential oil-loaded MOFs for food packaging. International Journal of Biological Macromolecules, 250, 126176. https://doi.org/10.1016/j.ijbiomac.2023.126176

Yong, Y., Wang, S., Li, L., Li, R., Ahmad, H. N., Munawar, N., & Zhu, J. (2023). A curcumin-crosslinked bilayer film of soy protein isolate and chitosan with enhanced antibacterial property for beef preservation and freshness monitoring. International Journal of Biological Macromolecules, 247, 125778. https://doi.org/10.1016/j.ijbiomac.2023.125778

Yuan, L., Liu, R., Zhou, Y., Zhang, R., Chen, S., Yang, Q., Gu, Y., Han, L., & Yan, B. (2024). Janus biopolymer nanocomposite coating with excellent antibacterial and water/oxygen barrier performance for fruit preservation. Food Hydrocolloids, 149, 109528. https://doi.org/10.1016/j.foodhyd.2023.109528

Zhao, L., Zhang, M., Mujumdar, A. S., & Wang, H. (2022a). Application of carbon dots in food preservation: A critical review for packaging enhancers and food preservatives. Critical Reviews in Food Science and Nutrition, 7, 1–19. https://doi.org/10.1080/10408398.2022.2039896

Zhao, L., Zhang, M., Wang, H., & Devahastin, S. (2022b). Effect of addition of carbon dots to the frying oils on oxidative stabilities and quality changes of fried meatballs during refrigerated storage. Meat Science, 185, 108715. https://doi.org/10.1016/j.meatsci.2021.108715

Zhu, Z., Meng, L., Gao, Z., Liu, R., Guo, X., Wang, H., & Kong, B. (2024). Development of chitosan/polycaprolactone-thymol Janus films with directional transport and antibacterial properties for meat preservation. International Journal of Biological Macromolecules, 268, 131669. https://doi.org/10.1016/j.ijbiomac.2024.131669

Supplementary

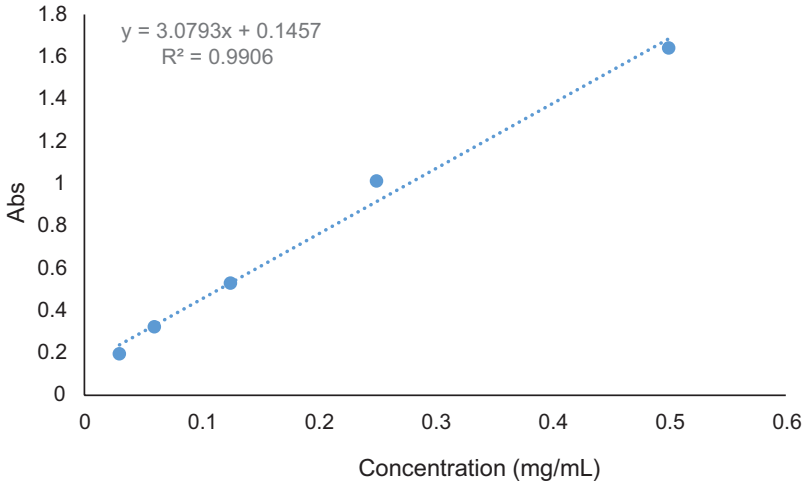

Figure S1. Calibration curve of JNPs release pattern at 280 nm

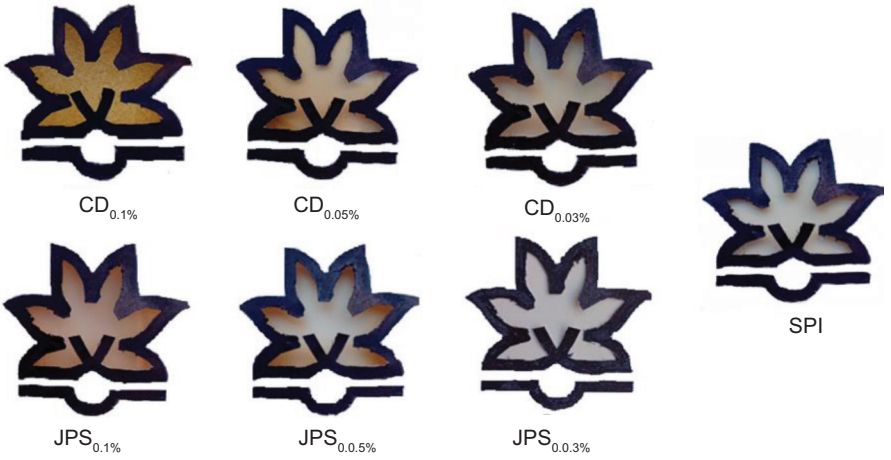

Figure S2. Photographic images of the SPI, SPI-CDs, and SPI- JNPs (0.03%, 0.05%, and 0.1%) (B).

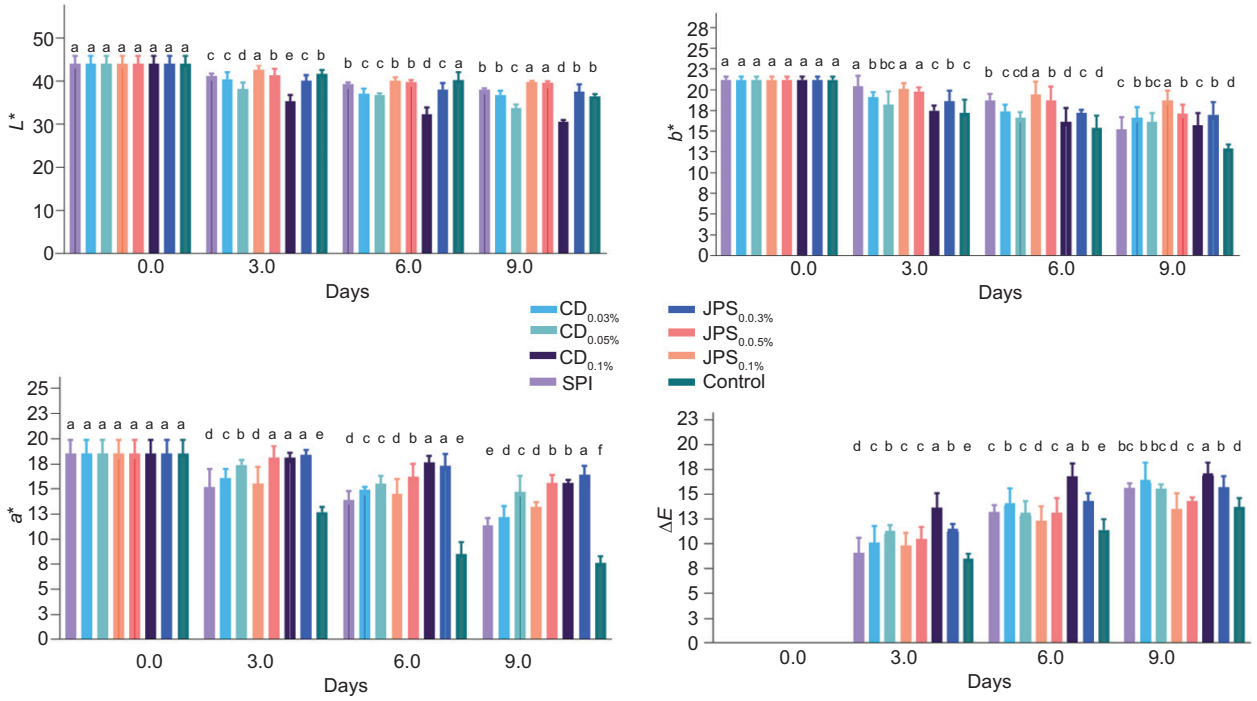

Figure S3. Color changes and color difference of meat packaged with SPI films, SPI-CDs, and SPI-JNPs films (0.03%, 0.05%, and 0.1%) during storage at 7 °C. Different letters within each concentration indicate significant differences ($p < 0.05$).

Table S1. The color (*L, *a**, and *b**) of SPI, SPI-CDs, and SPI-JNP films.**

Films	*L**	*a**	*b**	ΔE
SPI	84.1 ± 1.2^{a}	0.4 ± 0.9^{c}	18.7 ± 0.5^{e}	22.6 ± 1.4^{e}
SPI-$CD_{0.03\%}$	77.5 ± 0.7^{bc}	0.8 ± 1.5^{c}	21.5 ± 0.4^{de}	25.8 ± 0.6^{d}
SPI-$CD_{0.05\%}$	75.1 ± 0.9^{cd}	1.7 ± 1.3^{b}	24.2 ± 0.5^{c}	32.6 ± 1.1^{b}
SPI-$CD_{0.1\%}$	65.4 ± 0.8^{e}	3.2 ± 0.6^{a}	36.3 ± 1.3^{a}	48.2 ± 0.5^{a}
SPI-$JNP_{0.03\%}$	73.9 ± 1.3^{d}	0.6 ± 0.8^{c}	19.1 ± 1.5^{de}	34.1 ± 0.7^{b}
SPI-$JNP_{0.05\%}$	85.3 ± 0.5^{a}	1.3 ± 1.6^{b}	22.4 ± 0.6^{c}	27.7 ± 1.9^{cd}
SPI-$JNP_{0.1\%}$	80.2 ± 1.7^{b}	2.8 ± 0.5^{a}	28.5 ± 1.2^{b}	30.3 ± 0.5^{bc}

Within each column, values with different letters are significantly different ($p < 0.05$).